

NEW CONCEPTS IN ECHOCARDIOGRAPHY

Rotterdam, mei 1972

NEW CONCEPTS IN ECHOCARDIOGRAPHY

Proefschrift

ter verkrijging van de graad van doctor
in de geneeskunde aan de Medische
Faculteit te Rotterdam, op gezag van de
dekaan Dr. J. Moll, hoogleraar in de faculteit
der geneeskunde, tegen de bedenkingen
van het college van dekanen uit de
faculteit der geneeskunde te verdedigen
op woensdag 24 mei 1972 te 16.00 uur

door

Nicolaas Bom

geboren te Velsen in 1937

Promotoren : Prof. Dr. G. van den Brink
Prof. P. G. Hugenholtz

Co-referenten: ir. D. W. van Wulfften Palthe
Dr. M. de Vlieger

CONTENTS

	page
CHAPTER I INTRODUCTION TO ECHOCARDIOGRAPHY	9
1. General remarks	9
2. Purpose of this study	10
CHAPTER II PRINCIPLES OF ULTRASOUND	12
1. The piēzo-electric effect	12
2. Some physical properties of ultrasound	13
a. Attenuation	13
b. Reflection of sound	13
c. Near and far field	13
3. Scanning and recording techniques	15
a. Example of depth sonar	15
b. A-scan and Time-Motion recording	17
c. Single element B-scan techniques	17
4. The Doppler effect	17
CHAPTER III PRESENT APPLICATIONS IN CARDIOLOGY	19
1. General remarks	19
2. Mitral stenosis	20
3. Pericardial effusion	23
4. Other applications	26
a. Mitral insufficiency	26
b. Tricuspid stenosis	26
c. Idiopathic hypertrophic subaortic stenosis	26
d. Aortic valve study	26
e. Internal dimensions	27
5. On the use of Doppler	28
6. Concluding remarks	32

	page
CHAPTER IV A NON-INVASIVE METHOD FOR TWO DIMENSIONAL INSTANTANEOUS OBSERVATION OF MOVING CARDIAC STRUCTURES	34
1. Introduction	34
2. The system	35
3. Preliminary results	38
a. <i>Radiated intensities</i>	38
b. <i>In vitro and in vivo measurements</i>	39
 CHAPTER V A CATHETER TIP INTRACARDIAC SCANNER	 44
1. Introduction	44
2. The principle	45
3. On the selection of parameters	48
a. <i>Limits due to medical considerations</i>	48
b. <i>Limits due to production problems</i>	48
c. <i>Acoustic and electronic limitations</i>	48
4. The directivity pattern	49
5. Preliminary results	53
6. Concluding remarks	54
 CHAPTER VI ON THE LIMITATIONS OF ULTRASOUND	 56
1. Specular reflections	56
2. Range precision and axial resolution	57
a. <i>Range precision</i>	57
b. <i>Axial resolution</i>	58
3. Lateral resolution and effects caused by side lobes	60
a. <i>Lateral resolution</i>	60
b. <i>Side lobe effect in the non-invasive system</i>	61
c. <i>Side lobe effect in the intracardiac scanner system</i>	63
4. Limitations of continuous wave Doppler systems	64

	page
APPENDIX A THE MEASUREMENT OF ACOUSTIC RADIATION (The calibration of a sensor)	66
1. Introduction	66
2. Method of calibration	66
3. The sensor	67
4. Measurement of total output power	67
5. Calculation of intensity in a single position	68
6. Discussion of results	71
APPENDIX B THE MEASUREMENT OF ACOUSTIC RADIATION (The calculation of radiated power)	72
1. Introduction	72
2. Calculation of radiated power	72
3. The approximation	75
APPENDIX C PERICARDIAL EFFUSION. CASE REPORT	78
APPENDIX D MITRAL STENOSIS. CASE REPORT	82
APPENDIX E SIDE LOBE EFFECTS OF A LINE TRANSDUCER ON A CIRCULAR REFLECTOR ECHOGRAM	85
APPENDIX F OPTIMUM BEAM FORMING FOR INTRACARDIAC SCANNER	87
APPENDIX G POSSIBLE METHOD FOR DOPPLER MONITOR- ING	92
REFERENCES	93
SUMMARY	98
SAMENVATTING	99
NASCHRIFT	100
CURRICULUM VITAE	100

CHAPTER 1 INTRODUCTION TO ECHOCARDIOGRAPHY

1. General remarks

If short pulses of high frequency sound are transmitted through the heart, discontinuities in the tissues will produce reflected sound waves or "echoes". There will be a delay between a pulse transmission and the arrival of a corresponding echo. Together with knowledge of sound velocity this will enable determination of the distance between the transmitter/receiver and the reflecting interface, thus providing information about cardiac dimensions. Similarly the Doppler effect can be used to provide further diagnostic information. These applications of ultrasound (echocardiography) for the detection of cardiac (mal)function have recently gained acceptance even though interpretation of the information obtained can be difficult.

Major reasons for this acceptance are probably that, while the techniques provide information that otherwise is not available, most of the applications involve non-invasive methods and are well tolerated by the patient. In addition reports in the literature^{1,2,3} indicate that, at diagnostic intensity levels, the technique seems to be free from hazard.

The mitral leaflet motion recording and registration of movements of other cardiac structures as well as detection of relative changes in vascular blood flow are among the goals of echocardiography. Another aim is the determination of cardiac dimensions in order to derive intracardiac volumes, changes in wall thickness etc. While motion study involves a relative measurement, diagnosis based on dimensional studies calls for a precise image of the echo reflecting structure on the display, and thus is more difficult. Some of the reasons why ultrasound methods have thus far been used on a limited scale only are the limitations set by Nature (resolution in the order of a few millimeters, specular reflections, multiple echoes, etc.). Further difficulties may arise in the interpretation of the image and through lack of familiarity with the technique.

The first, practically useful, results with ultrasound diagnosis of abnormalities in human structures date back to the years between 1945–1950. The first in vivo application in cardiology was reported by Edler and Hertz⁴ in 1954. They applied a transducer to the human chest in the third and fourth intercostal space at the left border of the sternum and reported echo motion synchronous with heartbeat. After this discovery, ultrasound became recognized, step by step, as a diagnostic tool in cardiology. Since then several techniques have been described in the literature and some have become standard applications (see chapter III).

2. Purpose of this study

The moving heart within the body is a very complicated structure. While Leonardo da Vinci in the 16th century already proposed to register cardiac motions from needles stuck through the cardiac wall, (see figure 1-1), it was mainly through the indirect means of external palpation that clinicians tried to record its movements.

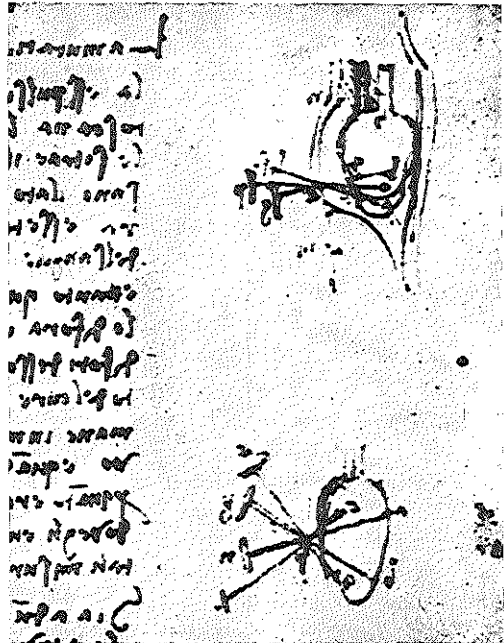


figure 1-1
Cardiac motion shown by
needles. A method sug-
gested for studies in pigs
in the 16th century by
Leonardo da Vinci.

Later, when roentgen rays became available, cardiac dimensions came within reach of objective assessment, but fluoroscopy remained a difficult art. It was only after 1955 when image amplifiers became available to reduce the X-ray dosage and when contrast media injected within the cavity brought modern angiocardiology within reach of the larger medical centers that the in vivo study of internal cardiac dimensions became possible to the extent that no modern cardiac center today could do without it.

We are now faced with a need for frequent examination of the moving heart in the intensive care unit. An important fraction of the examination techniques is based on the measurement of indirect parameters, for instance the electrocardiogram. Even though well developed, these methods do not provide the direct visual display of the moving heart. Continuous X-ray would be unduly dangerous. Thus ultrasound would seem an attractive alternative.

Thus far with current ultrasound methods real time information has been obtained only from a number of isolated structures in the heart. If it were possible to extend present methods to an instantaneous viewing of an entire cross-section of the heart, important additional diagnostic information might be provided. In order to approach this goal, the investigations reported in this study were carried out.

CHAPTER II PRINCIPLES OF ULTRASOUND

Summary:

The piëzo-electric effect used for sound to voltage conversion is explained. A brief description of some physical properties of ultrasound wave propagation is then given. Echo display and recording techniques will be described. An explanation of the Doppler effect for recording of blood flow concludes this chapter.

1. The piëzo-electric effect

The piëzo-electric effect, which was first discovered by Jacques and Pierre Curie in 1880, occurs in some materials when an electric field is applied in a certain direction. An element, formed from such material, becomes mechanically strained. The amount of strain is proportional to the intensity of the applied field. This effect is reversible. In figure 2-1 a rectangular element is shown. The element is covered on both sides with a thin silver electrode with which the electric field is applied. For

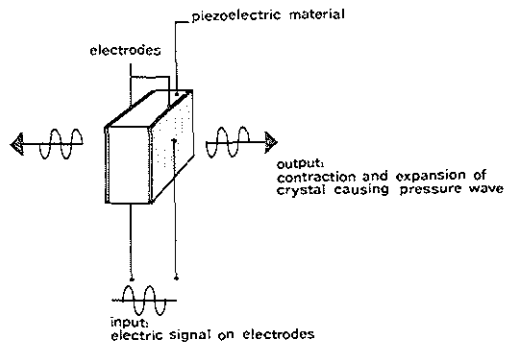


figure 2-1
The piëzo-electric effect.

proper resonance the elements have usually been cut to a special resonant size. Figure 2-1 shows, in a simplified way, that an applied electric pulse will be converted into a corresponding pressure pulse. By proper transducer positioning, this sound pulse may be aimed in the desired direction. Upon return, the echo causes the reverse effect and

thus the echo pressure wave causes a corresponding electric effect on the electrode wires. The piëzo-electric effect is used in many applications. A well known use is the "ceramic" gramophone pick-up element. In almost all applications of ultrasound the tip of the "transducer" is formed of such a piëzo-electric material.

2. Some physical properties of ultrasound

Sound with a frequency beyond the audible frequency is usually called ultrasound. Ultrasound in the 1 to 10 megahertz range is used for diagnostic purpose. Important properties are:

a. Attenuation

The intensity of a propagating sound wave in tissue diminishes due to absorption of energy by the tissue. The absorption increases with frequency. For muscle tissue it ranges around 1 db/cm/MHz, while in bone it is higher. This is the reason for selection of "low" frequencies if the sound has to propagate through bone or if deep penetration is required. In spherical propagation, the intensity of the sound wave diminishes proportionally with the square of the distance from the source. The energy in the sound wave is spread over an increased surface and this provides another cause of intensity decrease in a propagating sound wave.

b. Reflection of sound

The acoustic properties of the medium through which the sound travels may be expressed by its acoustic impedance.⁵ The acoustic impedance is defined as the product of density and sound propagation velocity. Reflection of ultrasound will occur whenever there is a change in acoustic impedance of the tissue through which the sound propagates. The reflection strength of the boundary depends on the difference in acoustic impedance of the two media. Under normal conditions some of the energy contained in the sound wave will be converted into echo energy at each reflecting boundary. For example, Reid⁶ measured reflection amplitudes of excised mitral leaflets in a watertank relative to a perfect reflector at the same range. For a normal leaflet a 38–39 db reflection loss was measured. For a heavily calcified valve the loss was between 18–30 db. Apparently a calcified leaflet is a better reflector.

c. Near and far field

In figure 2-2 the width of the sound field from a disk-shaped transmitter with radius r is shown. In the close vicinity of the transmitter the sound is confined to a cylindrical area. In this "near field" zone interference

occurs between sound waves coming from different parts of the transducer face. Thus in the near field a point reflector would cause echoes of varying strength depending on relative position. This may render echo detection difficult. In the far field this problem does not arise. Here the sound field is homogeneous and spreads spherically. Distance D (the distance of gradual transition from near to far field) is defined by $D \approx r^2/\lambda$ where r is the transducer radius and λ is wavelength. As an example, for a transducer element with a diameter of 1 cm and with a frequency of 3 MHz $D \approx 5$ cm. In the far field the shape of the sound beam may be described by a directivity pattern. This directivity is a function of transducer geometry and frequency.

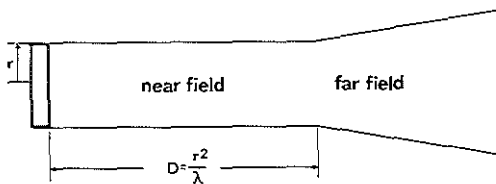


figure 2-2
Sound field in front of
radiator.

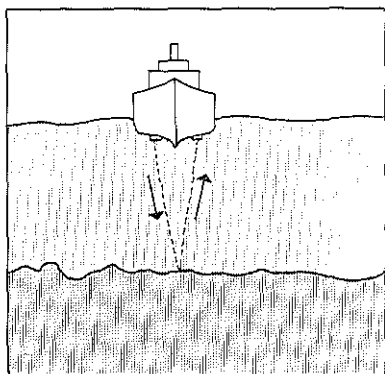


figure 2-3
Illustration of echo techniques by the
customary example of depth recording
by echo travel time measurement.

3. Scanning and recording techniques

a. Example of depth sonar

In this section the usual example of depth and fishery sonar is used to illustrate the echocardiographic method in a simplified way. Figure 2-3 represents a schematic drawing of a ship equipped with sonar. On its bottom a transmitting and a receiving element respectively transmits the sound pulse and receives the return echo.

Since the propagation speed of sound in seawater is 1500 m/sec, a bottom echo returning one second after transmission indicates a depth of 750 m. This process of pulse transmission and echo reception is repeated continuously. With this method, one is able to measure depth of bottom, schools of fishes or plankton layers.

In figure 2-4 a recording shows plankton layers in a bottom depth recording taken in the Mediterranean Sea. Each pulse transmission yields an "echo picture", which is drawn vertically. The horizontal scale represents time as the ship moves forward.

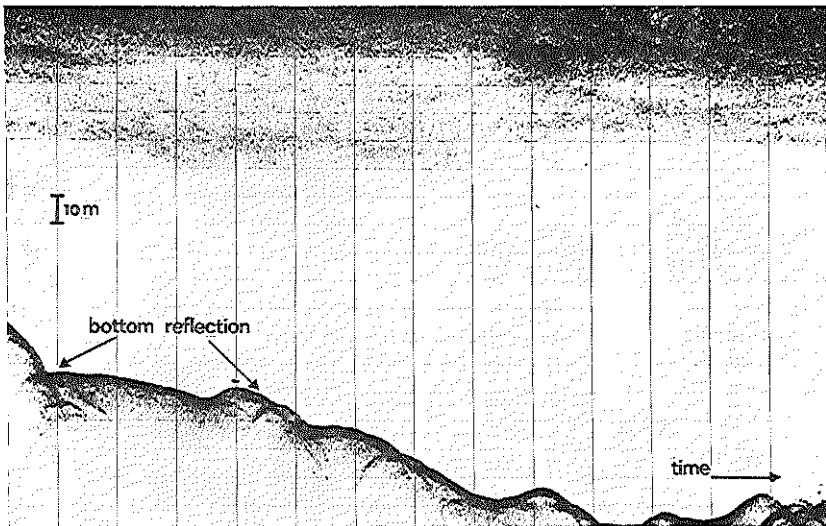


figure 2-4. Seabottom depth recording.

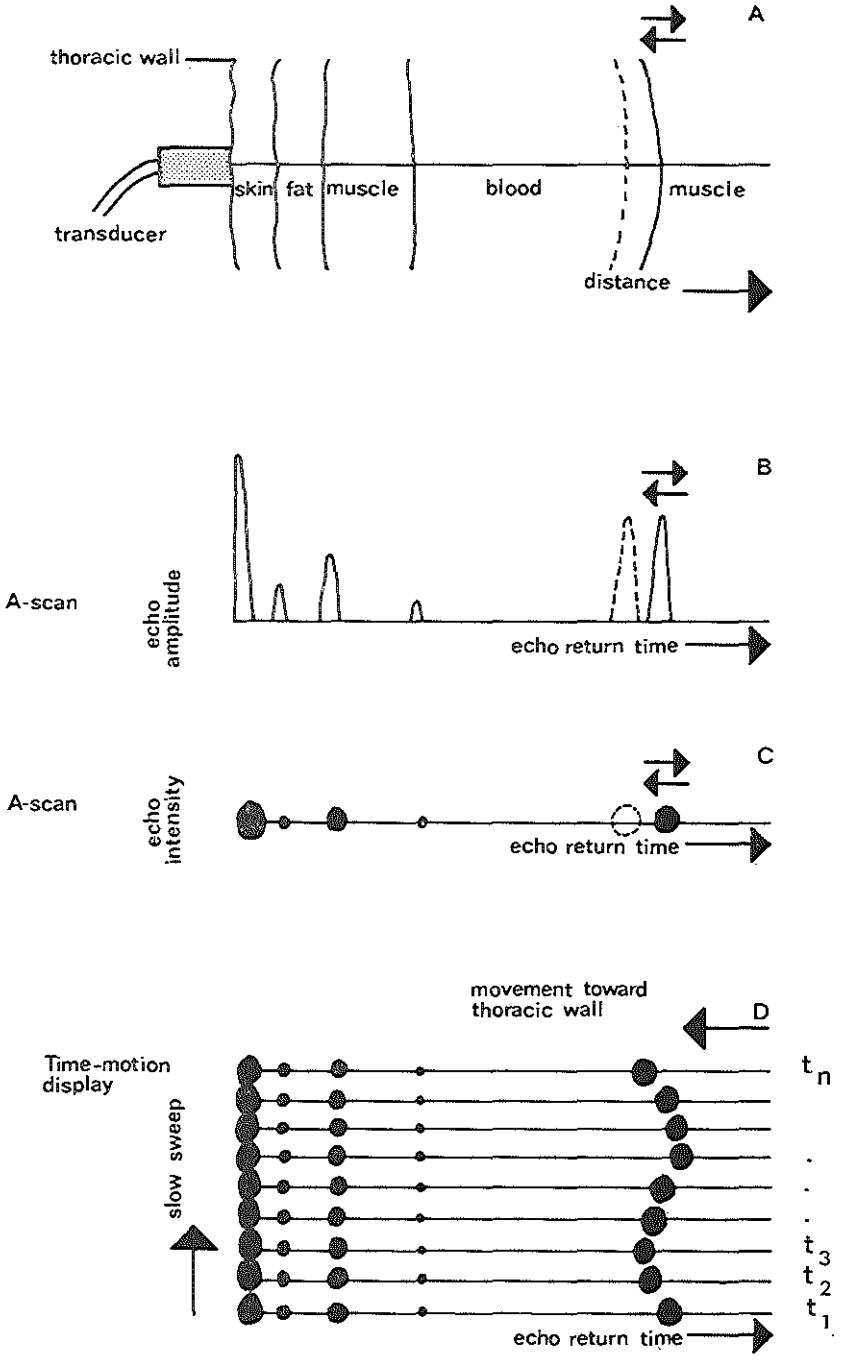


figure 2-5. Principle of A-scan and Time-Motion technique.

b. A-scan and Time-Motion recording

In single element echocardiographic techniques the transducer (transmitter = receiver) is held in a fixed position. Pulse transmission usually occurs every two milliseconds. Only one-dimensional echo structures in the sound beam can be visualized. The difference between A-scan and Time-Motion recording is just that of display (see below). In figure 2-5A the transducer position at the thoracic anterior wall is shown.

From left to right, at each change of acoustic impedance (blood/tissue, etc) part of the transmitted acoustic pulse energy is returned in the form of an echo. The echo height (figure 2-5B) may be displayed as a function of time on an oscilloscope. This is called the amplitude modulated A-scan. The echo height from each interface is a function of reflectivity, angle of incidence and path length.

Another possibility is the display of echo height as an intensity modulation on the oscilloscope. Here bright spots correspond to strong echoes. This is called intensity modulated A-scan (see figure 2-5C). If an echo originates at a moving interface, the spot will move correspondingly on the display (see figure 2-5A, B, C). The Time-Motion display is obtained when the intensity modulated A-scan is written on an oscilloscope with an added slow vertical beam deflection. For very long time intervals $t_1, t_2 \dots t_n$ this is illustrated in figure 2-5D. In practice, due to the high pulse repetition rate a continuous recording is obtained. The Time-Motion mode is thus a registration which is particularly well suited to the recording of the motion of structures. The recorded motion then represents the projection of the movement of a real structure motion in the sound ray path.

c. Single element B-scan technique

In B-scan an ensemble of parallel A-scans is displayed by successively moving the single transducer to an adjacent position. On the display depth is represented in X-direction with the Y-direction representing lateral position. In compound scanning the echo image is built up by aiming the transducer from different angles at the reflecting structure and deflecting the spot on the cathode ray tube through a corresponding angle. In this way geometrically correct two-dimensional information is preserved. In both techniques the final echogram may be built up photographically or on an oscilloscope memory tube. Since the mechanical transport of a single transducer element is time consuming these techniques are less suitable for application in cardiology.

4. The Doppler effect

A technique based on the Doppler effect is frequently used to obtain information concerning blood flow (see chapter VI, section 4). When

a sound wave is reflected back from a target, the frequency of the incident sound differs from that of the reflected wave by a quantity that is approximately proportional to the transmitted frequency and the relative velocity between the sound source and the reflector. The same principle holds for ultrasound reflected from erythrocytes in blood. The first applications of Doppler methods to measure blood flow were published by Franklin et al.^{7,8} and Satomura.⁹

Apparatus in general use today usually transmit a continuous ultrasound wave in the 1–10 MHz range. The probe contains two elements – one for transmission and one for reception – and may be applied on the outside of the skin or implanted. Figure 2-6 shows schematically the positioning of a transcutaneous probe over a blood vessel.

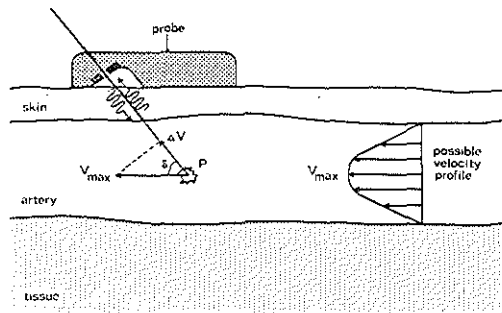


figure 2-6
Positioning of transcutaneous Doppler probe over artery.

The frequency shift can only be obtained from scattering particles in the sound beam of both transmitting and receiving element. Wells¹⁰ describes such directivity patterns and the geometry of the mutual zone. If this zone were limited to a small scattering volume around position P, only the frequency shift corresponding to ΔV would result. In practice information over the entire vessel diameter is obtained. With a velocity profile as shown, a Doppler spectrum around the transmitted carrier frequency will result. This spectrum contains the diagnostic information but must be down converted to a more accessible frequency range (see chapter III, section 5).

CHAPTER III PRESENT APPLICATIONS IN CARDIOLOGY

Summary:

Research on new clinical methods and development of related instrumentation, requires understanding of current ultrasound techniques and their limitations. A review of A-scan and Time-Motion recording in medical applications is given. The important mitral valve motion presentation and the ultrasonic detection of pericardial effusion are discussed in particular. Reference is made to clinical recordings. Two special cases out of a series of 110 patients with various cardiac malfunctions studied by ultrasound in our clinic so far are further described in appendix C and D. A brief discussion on present Doppler applications concludes this chapter.

1. General remarks

As explained in the previous chapter, the Time-Motion recording plays an important role in study of cardiac movements. This technique allows the recording of the motion of a single structure as well as the recording of the relative distance between different structures. If a single time gate and level detector is used (as is often the case), a single structure motion may be written on a paper recorder. Sometimes an oscilloscope with a storage tube is used. In this fashion the motion of more than one structure can be obtained simultaneously.

Almost all recordings are obtained with a transducer positioned in an intercostal area a few centimeters away from the left sternal border. As ultrasound is heavily attenuated by air, a position must be selected from which the heart can be reached with minimal interference from lung tissue. A new approach has recently been described by Goldberg,¹¹ who used a supra-sternal position for transducer application. This enabled him to measure the lumen diameter of the aortic arch, the right pulmonary artery and the left atrium. These measurements all assume that the proper origin of echoes can be identified.

In order to confirm the origin of mitral valve echoes, Edler et al¹² carried out a study whereby a needle was used to follow the sound path. This was done in an experiment in which the characteristic echo patterns were reconstructed in calf and cow hearts in a closed fluid system. During similar *in vivo* recordings Effert et al¹³ noticed the

absence of a late diastolic anterior motion (see section 2) in cases of atrial fibrillation or A.V.-nodal rhythm. They provided thereby further evidence that the echo had been caused by the anterior mitral leaflet. More recently, a very elegant study of echo recognition was carried out by Gramiak et al.¹⁴ He injected ultrasound reflecting contrast fluid (in particular indocyanine green which, when injected, apparently contains small air bubbles). During Time-Motion recording on the storage oscilloscope cavities were clearly outlined. This allowed perfect identification of echoes.

2. Mitral stenosis

Much attention in the literature is devoted to the evaluation of mitral stenosis with ultrasound. The first application was described by Edler and Herz⁴ in 1954. In mitral stenosis, the narrowed valve opening represents an obstruction to the blood flow. This may be caused by fibrotic thickening or calcification of the cusps or by adhesions between the cusps at the commissures. The echo technique for recording leaflet motion has been extensively described by many authors and will be briefly summarized here. The technique is based on the Time-Motion recording described in chapter II. In figure 3-1 the simplified geometry (schematic drawing after Gordon¹⁵) and transducer positioning is shown.

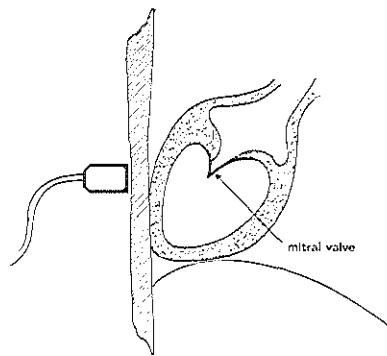


figure 3-1
Schematic view of positioning of probe for recording of mitral leaflet movement.

Figure 3-2 shows the electrocardiogram (e.c.g.), the ultrasound-cardiogram (u.c.g.) and a phonocardiogram obtained from a normal individual. In figure 3-2 an upward motion in the u.c.g. represents a movement of the anterior mitral leaflet toward the anterior thoracic wall. In position E the valve is fully open and the anterior leaflet is in its most anterior position. The period E-F is the first, rapid, filling phase, which tends to approximate the leaflets somewhat. The closure speed recorded during this period is normally used for evaluation of the severity of mitral stenosis. Following the P-wave in the e.c.g. further closure of the mitral valve takes place, manifested by the interval A-B in the u.c.g.

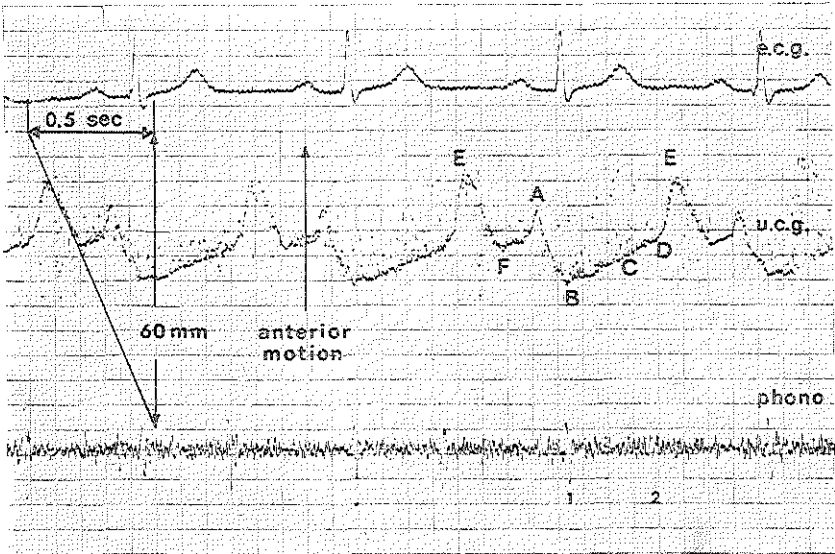


figure 3-2. Ultrasound cardiogram (u.c.g.) of anterior mitral leaflet motion in a normal individual.

The small anterior movement around position A is due to atrial contraction. Period A to B represents the late diastolic phase of filling and point B the actual closing of the mitral valve and the occurrence of the first heart sound. Ventricular systole and hence a closed mitral valve exists during the period B to C. Between C and D the second heart sound is heard representing closure of the aortic and pulmonary valves. As may be seen in figure 3-2 the closure speed was measured to be 120 mm/sec. In order to obtain these records the transducer is positioned in the 4th intercostal area, a few centimeters lateral to the left sternal border, and aimed in an anterior-posterior direction. Kossoff and Wilcken¹⁶ pointed out that from a single patient different values for the closure rate may be obtained. They showed in one patient a variation in leaflet excursion from 21 to 28 mm and a change in velocity from 63 to 120 mm/sec. It was pointed out that depending on the angle of the probe, different parts of the mitral valve may cause the reflection, leading to varying results. For diagnostic evaluation only maximum values are used. In figure 3-3 an u.c.g. is shown as obtained in a patient with severe stenosis. The movement becomes less abrupt with a closure speed of only 8 mm/sec in this case.

In the evaluation of the degree of severity of mitral stenosis from the u.c.g., the following characteristics are generally considered:

- the anterior leaflet diastolic closure speed,
- the leaflet excursion or amplitude and
- the echo thickness

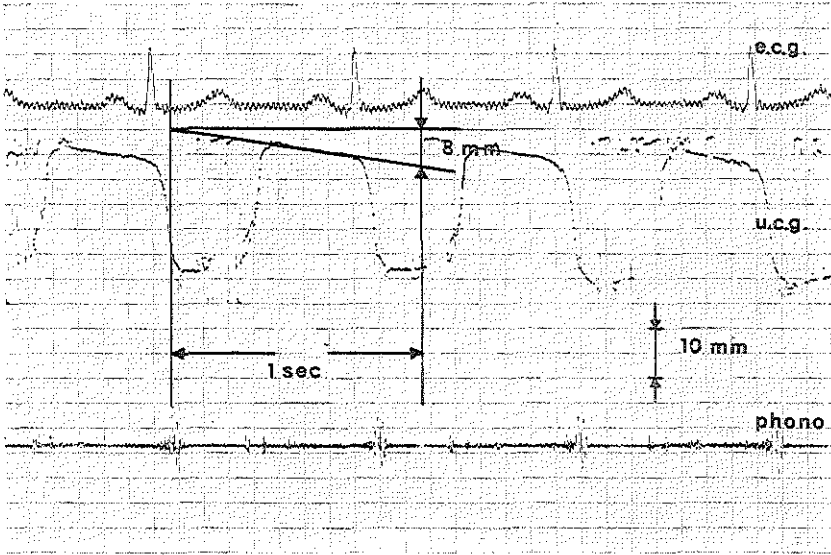


figure 3-3. Ultrasound cardiogram (u.c.g.) of anterior mitral leaflet motion in a patient with severe stenosis.

Figure 3-4 shows velocities indicating normal or stenotic mitral valves as given by several authors^{6, 13, 17, 18, 19}. No apparently significant difference exists between several authors' conclusions as to the relation between measured velocity and the degree of stenosis. In most cases the 35 to 50 mm/sec range is mentioned as a border-line situation of mild stenosis. Velocity decreases with increasing stenosis.

In a study on 2156 patients Effert et al¹³ report that in cases of extreme mitral stenosis (mitral valve area 0.8 cm² or smaller) in which the surgeon can just dip his fingertip into the valvular orifice, the rate is reduced below 10 mm/sec. In high grade stenosis (valve area 0.8-1.5 cm²), in which surgeon's fingertip can just pass the mitral orifice, closure rates between 10 and 25 mm/sec are found.

Although the data on the extent of the leaflet excursion are less specific, most authors agree that an amplitude in the 20 to 35 mm range may be considered as normal. Joyner et al^{19, 20} and Kossoff and Wilcken¹⁶ concluded that small amplitudes occur in patients with a thick fibrotic or calcified leaflet. A thin pliable leaflet will show a larger amplitude. The same observation has been described by Gustafson²¹ in a larger series of patients on whom confirmation by surgical data was available.

In the examples shown in figure 3-2 and 3-3, a time gate is used which allows for the selection and recording of just one echo. This procedure

enhances the clarity of the recording. If the Time-Motion recording is directly taken from a storage oscilloscope more detailed information about the reflecting structure may be available. Joyner observed a thick echo in cases of heavy calcification. Extensive measurements on excised leaflets were carried out by Reid.⁶ He studied the effect of leaflet thickness and angle of incidence on echo structure. He found that the thickness should be derived from echoes obtained in the most anterior position of the leaflet, since it is then perpendicular to the sound beam. Thickness measurements obtained at this position permitted the separation of normally pliable, moderately thick or extremely thick valve leaflets.

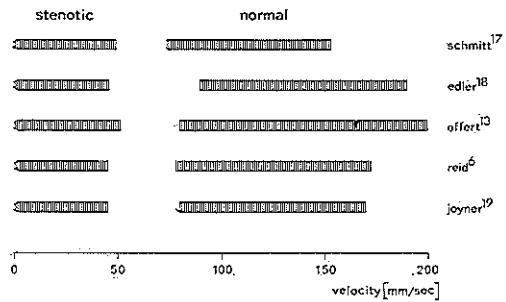


figure 3-4
Range of normal and stenotic mitral valve leaflet closure speeds as reported by several investigators.

The practical significance of the mitral valve evaluation with ultrasound may be revealed from the fact that in the clinic of Effert only 3 % of the patients with mitral disease undergo cardiac catheterization for the recording of intracardiac pressures, in all others u.c.g. constituted the main diagnostic test.

A study of the timing of opening snaps which are frequently heard in mitral stenosis, was carried out by Friedman.²² In most instances the opening snap occurred within 5 msec (his error of measurement) after the opening of the anterior mitral leaflet. This supports the hypothesis that the opening snap is caused as a result of the anterior position of the leaflet at that time.

3. Pericardial effusion

A generally accepted application is the detection of pericardial effusion. In this condition the pericardial sac is filled with fluid. The echo technique proved to be of particular value since it may be rather difficult to differentiate between a large heart or pericardial effusion, if X-ray techniques alone are employed. An early description of the technique has been given by Hertz and Edler²³ in 1956.

In figure 3-5A and B, the situation with and without effusion is shown schematically. This illustration shows a horizontal cross-section through the thorax with the transducer applied in the left sternal border area. The fluid in the pericardial sac causes an absence of strong echoes over the liquid filled interspace. This is the main feature of ultrasonic detection of effusion. Posterior-anterior X-ray photographs of the thorax before and after operation for removal of the fluid are shown in figure 3-6 and 3-7. From this patient 1800 cc of fluid was removed. (The case report is given in appendix C). The corresponding echograms are shown in figure 3-8.

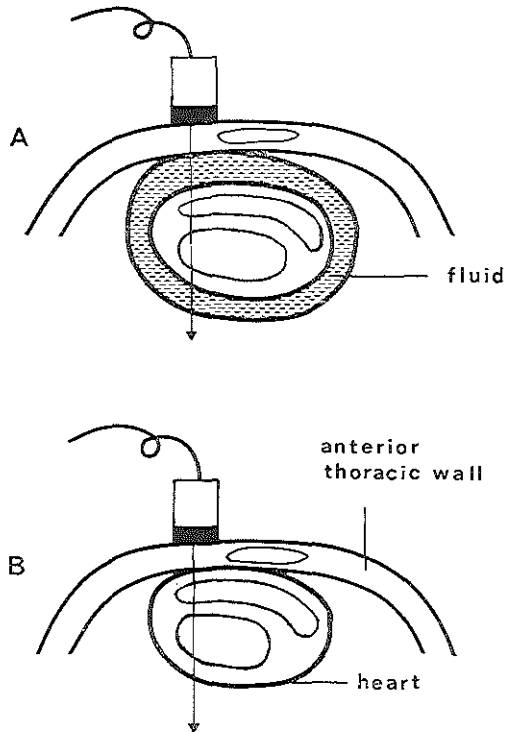


figure 3-5
A schematic view of the cardiac geometry in a patient with and without effusion. The dotted area indicates the zone with relative absence of echoes in the situation when an excessive amount of fluid fills the pericardial sac.

The relative absence of echoes from the fluid filled zone (see figure 3-8A) and the change after operation (fig. 3-8B) are clearly shown. Less clear perhaps is the abnormal and excessive excursion when effusion is present (A) as compared to a normal excursion after drainage (B). Excessive cardiac motion in some patients with severe effusion has been described by Feigenbaum et al.²⁴ On the other hand a reduction in cardiac motion in patients with acute tamponade is fairly common. Under these acute circumstances the pericardium cannot be expected to stretch much. Feigenbaum concluded therefore that only in long standing pericardial disease there will be sufficient stretching of the pericardium to permit the heart to move freely or even overactively. In agreement with this hypothesis are the available X-ray thorax photographs of the patient under discussion. These photographs show a

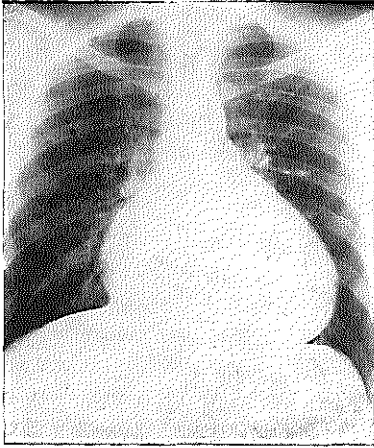


figure 3-6
Posterior-anterior X-ray photograph of the thorax in a patient with severe pericardial effusion. Note the degree of cardiac enlargement.

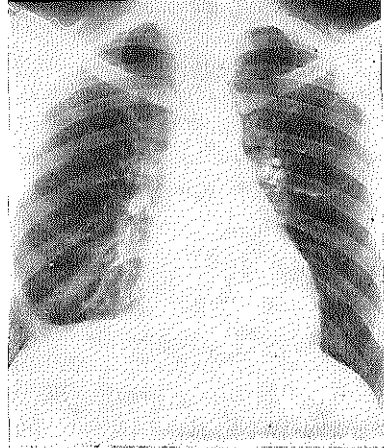


figure 3-7
Photograph of thorax roentgenogram of the same patient after removal of 1800 ml of fluid.

gradual increase in heart size over the three years prior to admission and studies shown in figure 3-6, 3-7 and 3-8. In another publication Feigenbaum et al²⁵ describe the effect of saline injection in the pericardial space on the echo pattern. In dogs the artificially induced effusion could be detected at the anterior heart wall or at the posterior heart wall/lung interface. Joyner²⁶ reported the detection of effusion at the posterior wall to be easier. However, fluid may be detected erroneously if, for instance, the more anterior mitral ring echo is taken for the posterior heart wall echo.

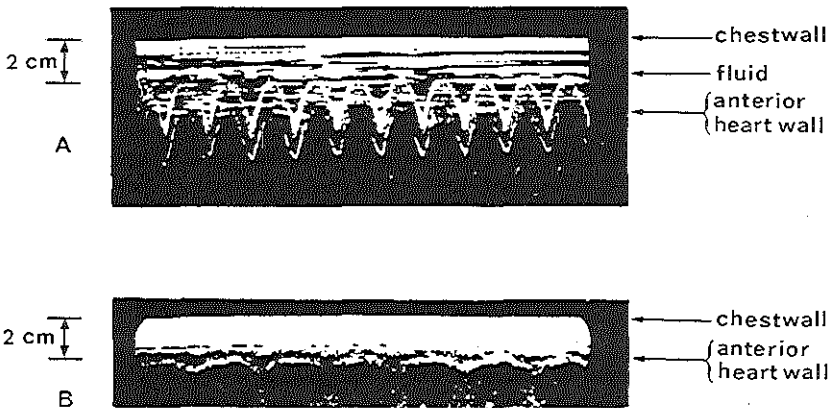


figure 3-8. Recording of anterior heart wall motion in a patient with pericardial effusion (A) and after removal of fluid (B). Note the relative echo absence in the fluid filled area and the excessive anterior cardiac wall movement.

4. Other applications

a. *Mitral insufficiency*

An increase in amplitude of the mitral u.c.g. and an increase in the closure speed has been taken as an indication of pure mitral insufficiency. However, in a recent article by Werning²⁷ it is once more pointed out that confusion with normal u.c.g.-recordings may occur.

b. *Tricuspid stenosis*

Recording of the tricuspid valve u.c.g. is not as easy as the mitral u.c.g. Gibson et al²⁸ describe the u.c.g. in tricuspid stenosis, a relatively rare disorder. The records were obtained from the same transducer location as the mitral u.c.g. transducer position. The characteristic echo motion resembles that known of mitral echo motion. The echoes are found more medially and anterior to the mitral echo. Joyner et al²⁹ report that the tricuspid curve is most easily recorded from individuals who have pulmonary hypertension or any condition which results in rotation of the heart into a more vertical and anterior position.

According to Joyner, the closure velocities derived from the tricuspid u.c.g. in normals are somewhat below those for the mitral closure speed (60–125 mm/sec).

c. *Idiopathic hypertrophic subaortic stenosis*

A differentiation between idiopathic hypertrophic subaortic stenosis (I.H.S.S.) and valvular stenosis is described by Moreyra et al.³⁰ These authors compared the mitral u.c.g.-recording in 16 patients with I.H.S.S. to the u.c.g. of 25 patients with valvular aortic disease. It was noted that in almost all cases of I.H.S.S. the mitral echo in its most anterior position merged with the septal echoes. Popp et al³¹ noted an additional abrupt anterior motion in the mitral u.c.g. during systole. The same abnormal systolic anterior motion in case of I.H.S.S. was noted by Pridie et al³² and Shah et al.³³

d. *Aortic valve study*

In a recent publication, Hernberg, Weiss and Keegan³⁴ describe the technique for u.c.g.-recording of the aortic valves. Their experience shows that in a high percentage of those patients whose mitral valve echo can be obtained, the aortic valve recording is also possible. Moderate to severe aortic valvular disease makes it, however, extremely difficult to obtain meaningful echoes from the aortic region. Gramiak et al¹⁴ demonstrate clear recordings of the aortic root and leaflet motion. Both Hernberg and Gramiak³⁵ found that absence of normal systolic cusp motion is a reliable indication of aortic stenosis.

Premature closure of the mitral valve as seen in the mitral u.c.g., was described by Priddle et al³⁶ as a reliable sign for the detection of aortic regurgitation. They found that in these cases premature closure occurs up to 0.2 sec before the Q-wave. In a number of cases with aortic regurgitation they also noted diastolic oscillations on the mitral u.c.g. These were absent when mitral stenosis was present. Similar fluttering was reported by Winsberg et al.³⁷

e. Internal dimensions

Chapelle et al³⁸ measured systolic diameter (S.D.) and diastolic diameter (D.D.) of the left ventricle. Normally if only the mitral valve u.c.g. is used, some difficulties in differentiating between normal subjects and patients with mitral insufficiency may arise. Chapelle shows that when $(D.D.-S.D.)/S.D.$ is plotted versus mitral closure speed, distinction can be made between normal hearts, hearts with a stenotic mitral valve and hearts with an insufficient mitral valve. Furthermore considerable decrease in maximum posterior wall motion as measured during systole was noted in patients with cardiomyopathy.

A number of authors used the echo technique for the measurement of left ventricular internal dimensions. Feigenbaum et al³⁹ correlated these data to angiographically obtained dimensions and found, for instance, the correlation coefficient for the long axis to be 0.86. Pombo et al^{40, 41} used such data for calculation of stroke volume and Popp et al^{42, 43} extended these measurements to obtain information about the right ventricular size as well.

Left ventricular posterior wall thickness has been measured and reported by some authors. Feigenbaum et al⁴⁴ for instance measured the thickness of the left ventricular posterior wall. Between the echoes which were assumed to originate from the endocardium/blood interface and from the pericardium/pleura/lung interface, they found for the left ventricular wall in normal subjects a mean value of 1.1 ± 0.2 cm (range 0.8 to 1.3 cm). The importance of transmural wall thickness measurement was pointed out by Heikkilä et al.⁴⁵ In a study in which metal clips were used, they report that the rate of change in wall thickness is an excellent indicator of muscle function. Sjögren et al⁴⁶ compared ultrasonically obtained diastolic L.V. wall thickness with data derived from roentgen-films and found a correlation coefficient of 0.96.

In a recent publication Inoue et al⁴⁷ describe the measurement of the posterior L.V. wall excursion and posterior wall velocity in cases of acute and old myocardial infarction. Despite the rather small number of patients on which their data are based, it seems clear from this work that the reduction in amplitude of the posterior wall motion and the even

greater decrease in wall motion during systole were easily detected in patients with acute myocardial infarction. Compared to mean normal data as measured at rest by Kraunz et al⁴⁹:

Posterior wall excursion = 0.72 ± 0.18 cm
Posterior wall velocity = 4.1 ± 1.1 cm/sec

Inoue found in cases of acute myocardial infarction:

Posterior wall excursion = 0.54 ± 0.20 cm
Posterior wall velocity = 2.3 ± 0.9 cm/sec

Other applications have been mentioned in the literature. In general the accuracy in the distance measurements between different structures may not be as high as sometimes is suggested. For example the setting of radiated intensity or detection trigger level will strongly influence these measurements. For discussion on the influence of those factors on the resulting recording the reader is referred to chapter VI.

5. On the use of Doppler

As explained in the previous chapter, the shift of frequency and hence information on blood velocity may be obtained by frequency demodulation of a reflected ultrasound wave. Straightforward demodulation with the carrier frequency yields a Doppler spectrum in the audio range with loss of directional information. However, with the use of more complicated demodulation techniques directional information may be preserved. Throughout the cardiac cycle the velocity profile and consequently the Doppler spectrum changes rapidly. Since the instantaneous measurement and display of a spectrum involves complicated electronics, some commercial Doppler apparatus give a recorder output related to "average spectrum frequency". This signal may be recorded as a function of time and is sometimes indicated by the unfortunately chosen name "blood flow velocity" (see chapter VI). The audio signal contains more frequencies than such a written recording hence characteristic changes in the Doppler signal are more easily detected when using earphones.



figure 3-9
Doppler recording at the
brachial artery in a normal
individual.

The Doppler effect is further discussed in the example following. In figure 3-9 a Doppler recording obtained at the brachial artery in a normal individual is shown together with his electrocardiogram. The recording was obtained with a commercially available instrument and probe (Parks Electronics, Beaverton, Oregon, U.S.A.). In this instrument the directional information is preserved. The zero level was recorded by compressing the artery in a proximal position. The recording has an oscillatory character.

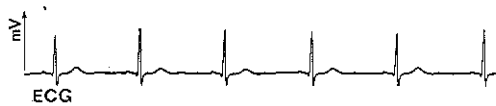
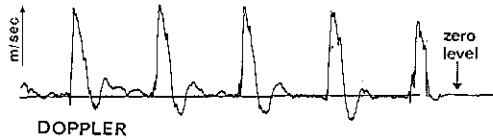


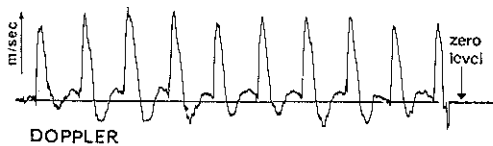
figure 3-10
Doppler recording at the femoral artery in a patient with severe aortic insufficiency.



This oscillatory character has been described as observed at different positions by Kalmanson,⁴⁹ Pourceiot⁵⁰ and others. Kalmanson related these findings to the work of McDonald.⁵¹ This investigator explained oscillatory flow by the instantaneous pressure gradient between two points in the femoral artery. He estimated that the reverse flow had already started during end-systole, and thus before aortic valve closure. This timing is important as providing a possible explanation of the blood reflux noted in the recording. Apparently the closure of the aortic valve is not the direct cause of the first reversal. That this may be true is shown in a comparison of a recording at the femoral artery in a case of severe aortic insufficiency (figure 3-10), and the recording at the femoral artery of a patient with coronary by-pass (figure 3-11).



figure 3-11
Doppler recording at the femoral artery in a patient with coronary by-pass and elevated heart rate.



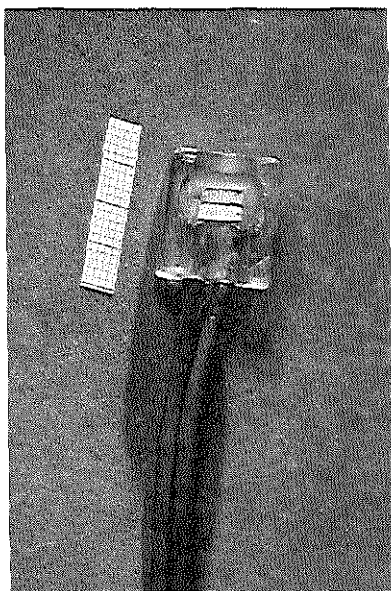


figure 3-12
Transcutaneous Doppler probe (Parks Electronics) with millimeter grid.

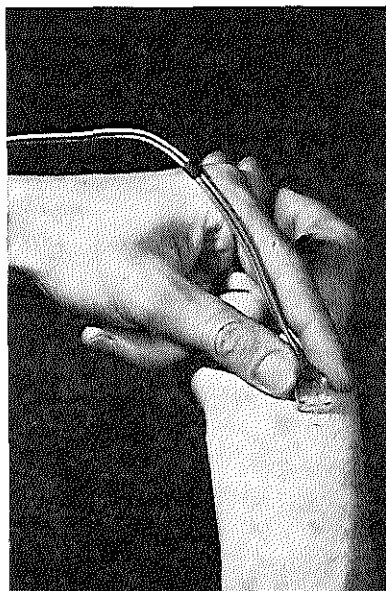


figure 3-13
Transcutaneous probe in position over the radial artery.

Apparently no increased reverse flow in the case of severe insufficiency can be demonstrated at the femoral artery. The same absence of increased reverse flow was noted by McCutcheon in 12 patients with aortic insufficiency (personal communication). The probe used is shown in figure 3-12 together with an example of probe positioning over the radial artery in figure 3-13.

Different types of probe can be used. For example a probe recently developed by our group in Rotterdam for use in open chested animal experiments is shown in figure 3-14. Probe size ranges from 3 to 20 mm diameter. After implantation it was sometimes necessary to wait a short period (up to half an hour) for development of proper acoustic coupling. No coupling gel was used, as body liquids apparently fill the element cavity slowly and thereby provide the necessary acoustic path.

The majority of Doppler applications mentioned in the literature concern the detection, location and follow-up of arterial and venous diseases in the lower extremities. Strandness et al,⁵² Sigel et al,⁵³ Allan et al⁵⁴ and others describe changes in pulse wave form between either side of an occlusion. A refined technique is described by Woodcock and Gosling.⁵⁵ They use two Doppler flow meters simultaneously in different positions. By spectral analysis of the arterial blood-velocity/time wave form, they

obtain information on what is called a “pulsatility” index. By measuring this index, a damping factor and the transit time it appeared possible to:

1. Produce a grading of collateral circulation
2. Obtain assessment of limb viability and
3. Distinguish between localized and generalized narrowing.

Benchimol et al⁵⁶ described the possibility of continuous monitoring of the dorsalis pedis artery in a coronary care unit. He noticed that in the presence of an unchanged e.c.g. the Doppler signal showed changes 30 to 60 minutes before the onset of severe left ventricular failure. Alexander et al⁵⁷ and Kalmanson et al⁵⁸ studied the venous blood flow in a number of cases with arrhythmias involving dissociation between atrial and ventricular activity. It was observed that the effect of both cardiac events – atrial relaxation and ventricular contraction – is necessary to achieve normal venous inflow. Other applications include a multi-channel Doppler blood flow system described by Rositano and Sandler.⁵⁹ This system has been used in animal studies and for the recording of Doppler signals on multiple arterial and venous sites in humans.

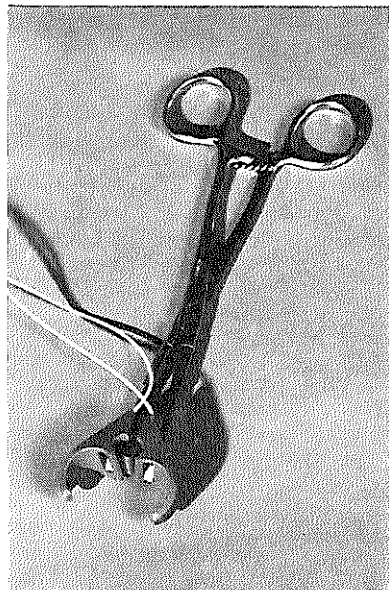


*figure 3-14
Pincher probe developed for implan-
tation around arterial vessels.*

So far attention has been paid to continuous wave Doppler systems only. Baker et al,⁶⁰ Flaherty et al,⁶¹ and Peronneau et al⁶² describe a new concept using pulsed Doppler systems. As in continuous wave situation the velocity is proportional to the frequency shift. Such information may

be also obtained from a pulse. In addition depth information may be obtained by time gating of pulses from a selected depth (travel time) only. The Doppler frequency shift is proportional to the transmitted frequency, therefore sensitivity to changes in velocity increases with frequency. Due to changes in absorption with frequency a better penetration is obtained with a low frequency system. These parameters constitute a design criterion for continuous wave Doppler techniques.

In the systems whereby pulses are used an additional compromise must be reached. First, penetration depth now becomes restricted by the repetition time. Secondly, a pulsed signal has a corresponding line spectrum around the carrier frequency. The distance between the carrier frequency and the first side bands decreases with the decreased repetition frequency. During analyses of Doppler shift any possible confusion with the side bands must be avoided. This then restricts the maximum measurable velocity.

With a pulsed system Peronneau obtained the instantaneous velocity profiles at different moments of the cardiac cycle and at different points in the aorta of dogs.

6. Concluding remarks

The motion of the anterior mitral leaflet as recorded by ultrasound seems to be used on a routine basis by a limited number of cardiologists. Recording of pericardial effusion may sometimes be easier but has potentially more pitfalls during analysis. Other applications (excluding Doppler) have been carried out on limited series of patients only, and, – with currently available A-scan single element systems – require much more experience. Measurement of motion of a structure, once identified, provides often valuable diagnostic data.

In addition, distance measurements between different structures may be carried out and seem to carry particular promise. However, these data should still be regarded with some reservation, as the settings on the apparatus will influence the echogram. As an example, no correct left ventricular internal diameter can be obtained if the septal echo is not “double” (i.e. an echo from right ventricular blood/septal boundary and the septal/left ventricular blood reflecting interface). Even then the problem of range precision remains (see chapter VI). The aim of the probe will further influence the measured length. Thus, recognition of the origin of echoes is one of the major problems in this field. At present a number of “landmarks” have been identified and are used

by clinicians. Amongst these are the mitral valve echo and the left ventricular posterior wall echo. In no way is it possible with current systems to obtain an overall view of moving cardiac structures. If possible, such a feature would make recognition considerably easier.

Transcutaneous continuous Doppler techniques offer an excellent method for diagnoses based on relative changes in blood velocity. However, no absolute information on volume flow can be obtained. More effort should be put into the spectral analysis of the complete shifted Doppler frequency spectrum since this contains more information compared to recordings from current apparatus that show an "average frequency shift" (see chapter VI, section 4). If monitoring is intended, a zero-crossing shift detection method might be useful (see appendix G). The pulsed Doppler system enables the measurement of velocity profile and thereby of volume flow. This may lead to a significant increase of information which cannot be obtained with current Doppler apparatus.

CHAPTER IV A NON-INVASIVE METHOD FOR TWO DIMENSIONAL INSTANTANEOUS OBSERVATION OF MOVING CARDIAC STRUCTURES

Summary:

In this chapter an ultrasonic scanner with twenty adjacent elements is described. The system has been designed to evaluate a non-invasive technique for visualizing moving cross-sections of the heart, particularly the walls of the ventricle. Fast electronic switching from one element to another and appropriate display of the echoes results in the instantaneous display of a moving structure. In vitro measurements are discussed. In vivo measurements are illustrated in a case of severe mitral stenosis.

1. Introduction

As mentioned in the previous chapter most clinical applications are based on systems in which a single element transducer is used. In one such method, the A-scan (see chapter II), a transducer is used in a fixed intercostal position to study the one dimensional tissue structure along the sound beam. Further development of this method to give a two-dimensional cross-sectional view requires more than one sound beam which in turn calls for physical movement of the transducer. Such a scan would obviously be considerably more informative than the A-scan. However, the necessary mechanical motion of the transducer is time-consuming and this has so far made it impossible to get an instantaneous cross-sectional display of the heart.

In the literature several attempts to obtain instantaneous non-invasive cardiac visualization with ultrasound have been described. Åsberg⁶³ obtained two-dimensional information of the heart over an arc of about 30 degrees. He used a mechanically rotated mirror system with a water bath contact. In doing so the information rate was limited to seven frames per second. Limited scanning rate and difficult transducer aiming are some of the problems associated with mechanical rocking systems sometimes mentioned in the literature.

The present state of a parabolic mirror system developed at Siemens was recently described by Pätzold et al.⁶⁴ In this system a small rotating element in an oil bath and a fixed reflector is used. Through a plastic foil, which encloses the oil bath, the ultrasound beam writes an echogram with an image rate of 16 frames per second. The dimensions of

this apparatus seem to make it more suitable to applications in obstetrics.

In sonar the use of element phasing to steer the main beam of a multi-element array has been known for many years. The first description of an application of this elegant technique in ultrasound was given by Somer.⁶⁵ No mechanical movement of the multi-element transducer is necessary due to rapid electronic change of the beam direction. Due to the delay line switching and the high ultrasound frequencies, the electronic circuitry of such systems requires a high degree of sophistication. His system was basically designed for use in neurology but might eventually be used in cardiology as well.

Some authors (Ebina et al,⁶⁶ Tanaka et al,⁶⁷ Robertson et al⁶⁸) suggest the stroboscopic effect for obtaining a cross-sectional picture from the heart. In such methods a single element is used. Sequentially at a pre-selected time of the cardiac cycle an A-scan is written (triggered by the electrocardiogram) on a storage display. Synchronism of transducer aiming and corresponding appropriate positioning of the echoes on the display results in a two-dimensional echogram. This picture then represents the heart as "frozen" at the selected time of the cardiac cycle. Making one picture requires many heart beats. Therefore, with these systems, no instantaneous two-dimensional viewing can be obtained.

In this chapter a method and preliminary results are described from a system in which an array of fixed elements rapidly scans the area to be explored, by means of electronic switching. Thus obviating any mechanical movement of a single element. With such a fast electronic scanner it is possible to produce an instantaneous echo pattern and thus display the anatomic structure without any "smearing" resulting from the movement of the heart. A comparable system has been suggested for use in ophthalmology by Buschmann.⁶⁹ He described a ten-element system whereby the single elements have been mounted in an arc to match the eyeball. A thorough review of the literature has failed to indicate the application of the switching principle to cardiology.

2. The system

Its principle is best summarized as "the use of n parallel A-scans at almost the same instant". A schematic drawing of a multi-element transducer is shown in figure 4-1.

The elements transmit a short acoustic pulse sequentially into the tissue. Returning echoes are displayed along a horizontal axis on the oscilloscope, while the vertical position of each line corresponds to the position

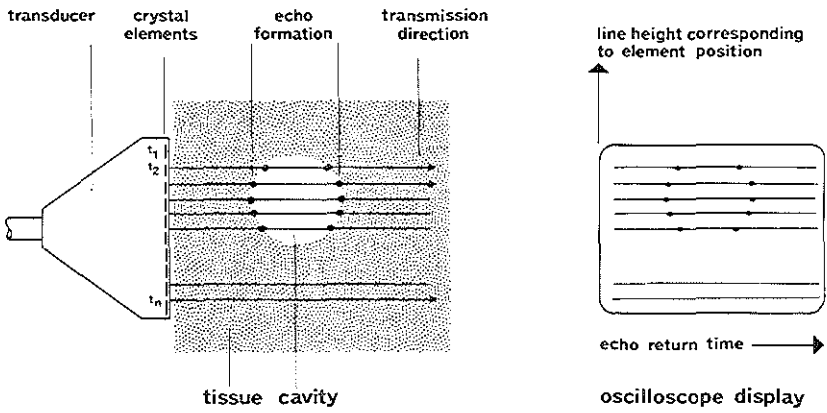


figure 4-1. Schematic drawing of a multi-element transducer and corresponding display.

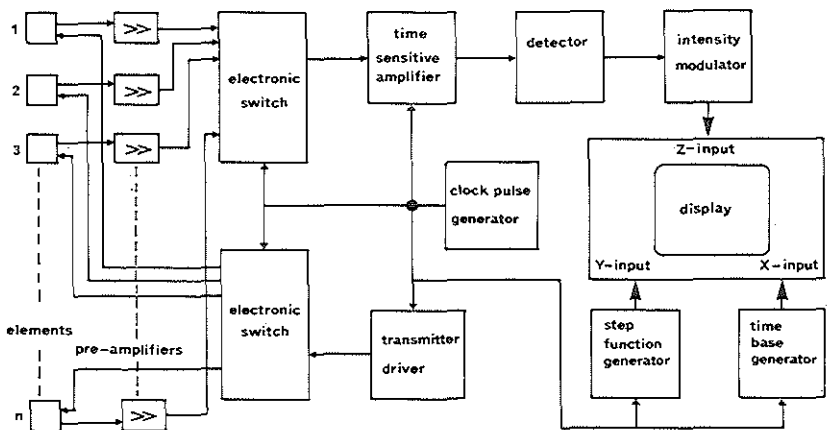


figure 4-3. Block diagram of an n -element system.

of the respective element. Under working conditions the horizontal lines are suppressed and only the echoes shown. Fast electronic scanning results in a repetition rate of 190 complete frames/second. An actual model of the transducer is shown in figure 4-2. With this transducer (front-length 6.6 cm) the displayed cross-section measures approximately 6 x 15 cm.

Limitations of this system (discussed in detail in chapter VI) are caused by poor resolution and specular reflections. As a result, with the present apparatus, only the viewing of gross movement of larger structures may be obtained. A block diagram of the principal components is given in figure 4-3.

In transmission a tone burst (a sinusoidal voltage of short duration at the resonant frequency of the crystal) is fed through an electronic switch into a single element. The element generates a short acoustic pulse. The echo signals arriving at this element when in the reception mode are amplified by a wide band pre-amplifier and fed through a switch into the processing part of the apparatus. This cycle is subsequently repeated for all elements. As the propagated sound is attenuated by spherical spreading and absorption in tissue, the first stage of the processing part contains a time dependent gain amplifier to compensate for these effects. The receiver gain is selectable as a function of the range. An envelope detector modifies the signal for the logarithmic intensity modulation circuit. This circuit displays the lowest and highest echo amplitude as respectively low and high intensity spots on the oscilloscope screen. The entire apparatus was first tested under in vitro working conditions as shown in figure 4-4.

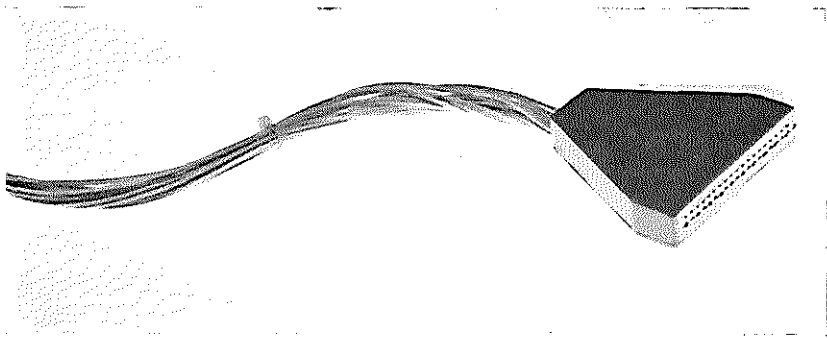


figure 4-2. A 20-element transducer (length 6.6 cm).

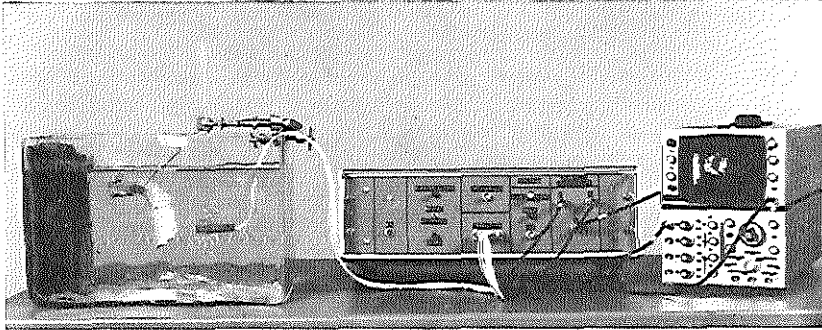


figure 4-4. The completed apparatus as used in an *in vitro* experiment. Shown is, from left to right: the water tank with aorta section and transducer, the apparatus, and the displayed cross-section on the oscilloscope.

3. Preliminary results

a. Radiated intensities

Since the apparatus has been developed for the display of moving structures, apparatus parameters, such as frequency and transducer size, have been chosen especially to suit applications in cardiology. A parameter of importance is further the radiated intensity (see page 66).

Low excitation voltage, required by the fast switching circuitry, has resulted in extremely low radiated intensities. These intensities were measured with the calibration probe as described in appendix A.

The intensity of radiation produced by the apparatus was measured, using the calibration probe at a distance of 6 cm from the multi-element transducer in the water tank. This depth was chosen because it corresponds to approximately the centre of the left ventricle when the transducer is applied at the fourth left intercostal space. In the case of a multi-element transducer as described, a position at 6 cm depth isinsonified by the sound from not only one but a number of elements. This is mainly due to the single-element beam width. Figure 4-5 shows the sound pulses that arrive at the calibration probe when it is positioned in front of element 7.

For proper calculation of the average acoustic intensity it is necessary to consider the sound pulse cluster as shown in figure 4-5, rather than the radiation from a single element alone. Using the calibration curve given for 3 MHz in figure a-6, the average radiated intensity is measured to be as low as 0.004 mW/cm^2 .

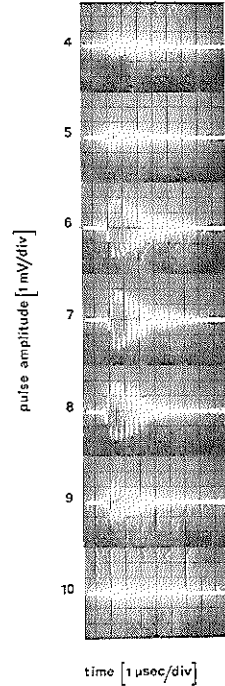


figure 4-5
 Cluster of sound pulses, from a number of elements, as received by the calibration probe when it is positioned at a distance of 6 cm in front of element 7.

From experience with the first prototype it soon became evident that with this intensity level reasonable results are obtained in thinner individuals only. Therefore, in near future an attempt will be made to increase the element excitation voltage.

b. In vitro and in vivo measurements

In general, a moving image is far better recognizable by the human eye than a still photograph. First experience, however, was obtained with echograms from non moving objects including excised hearts in the water tank. As an example the cross-section echograms of the aorta of a calf are given in figure 4-6 and 4-7.

It is evident that the approximate shape of the aorta is well recognizable. These echograms were obtained in an early stage where long pulse response of the time sensitive gain unit caused some image distortion. The echograms may be obtained in many ways. For instance height modulation may be coupled with modulation of the horizontal deflection voltage of the cathode ray tube to yield a quasi three-dimensional image. Such an echogram from a circular reflector was used on the cover page. In this chapter all further echograms have been of the simple intensity modulation type.

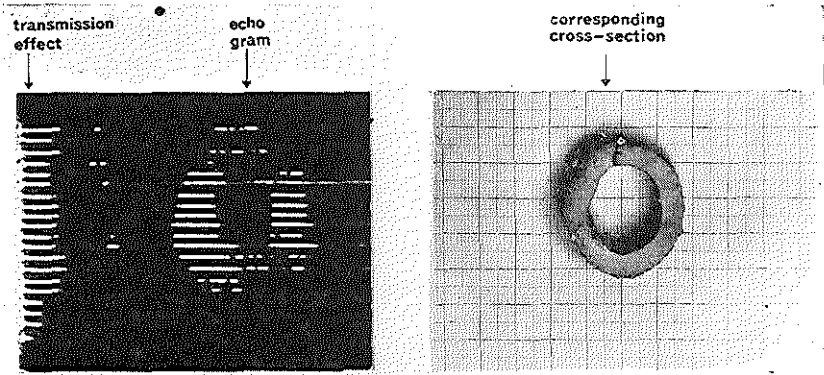


figure 4-6. Cross-sectional echogram of an aorta measured in vitro, and the corresponding segment of the aorta (scale in cm).

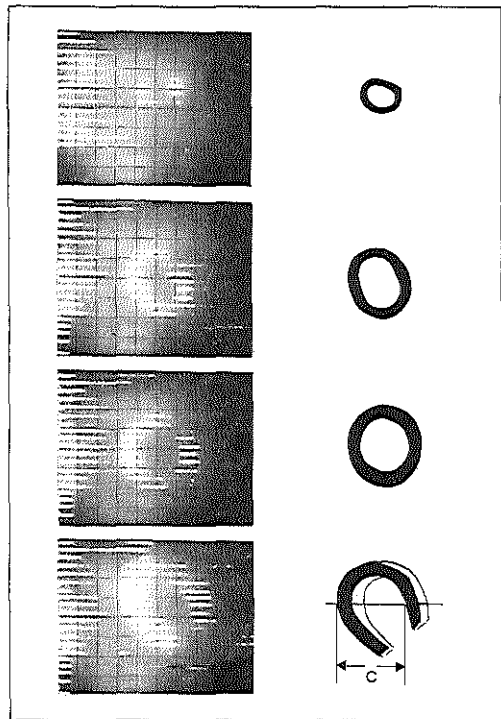


figure 4-7
Echograms of four aorta sections, each shown together with the corresponding "wet print".

More interesting are the results obtained so far in vivo on a small number of patients. With the transducer centered over the left fourth intercostal area, in most cases moving left ventricular structures such as posterior

and anterior walls have been recognized and displayed instantaneously and continuously. In the case of a patient with severe longstanding pericardial effusion (appendix C), the excessive motion of the entire anterior wall showed very clearly. The motion change after operative removal of fluid was apparent. An artificial valve could be viewed throughout the cardiac cycle in another patient.

As stated before, a moving image is better recognizable than a still photograph. As it is obviously impossible to illustrate this chapter with a moving film, an attempt was made to simulate this effect (see below) by showing a short sequence of echograms obtained from a patient with severe mitral stenosis and mitral insufficiency.

The transducer (in this case with 15 elements. Resonant frequency 4.5 MHz) was placed in a parasternal position at the left sternal border. In figure 4-8 one systolic frame of the echogram video recording and the corresponding sagittal section through the thorax and the heart are shown. The huge left atrium, confirmed later by cine angiography (see appendix D), and the left ventricular outflow tract are well recognizable. Most apparent from the video recording was the motion of the mitral leaflet and papillary muscles.

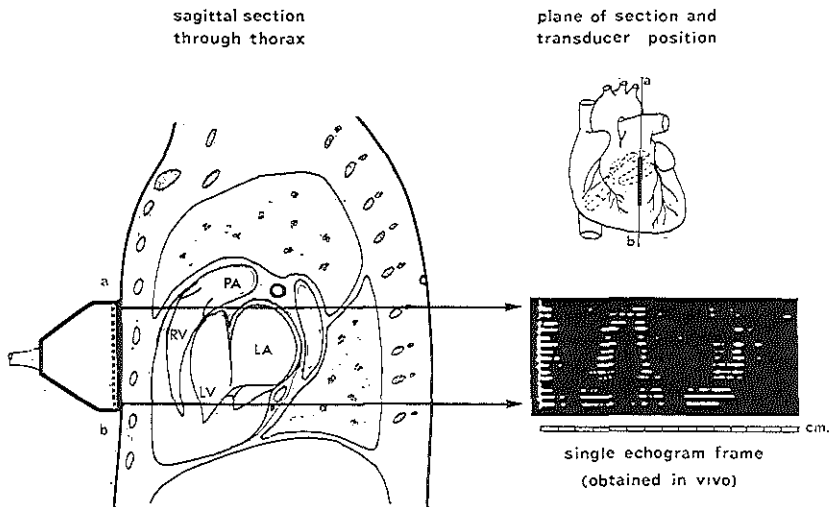


figure 4-8. Relation between transducer position, thorax and heart geometry and a resulting single frame echogram in a parasternal cross-section.

A short sequence of consecutive systolic cardiac echograms is shown in figure 4-9. The frames were obtained with an interval of 40 milliseconds. Utmost closure of the mitral valve is shown in frame T₆. As may be seen in frame T₁, 200 milliseconds earlier, the lower part of the mitral valve is in a more anterior position. It is further shown that the geometry of the L.V. outflow tract does not change significantly.

It is possible with this apparatus to select any single element from the multi-element transducer in order to obtain the conventional mitral valve motion recordings. The above described system would thus enable the study and identification of u.c.g.-recordings obtained from various parts of the leaflet. At present such a study has not yet begun. Once carried out the results will hopefully settle the controversy which sometimes arises on the origin of main motion components (motion of the heart and mitral ring plus leaflet motion) together yielding the accepted mitral leaflet u.c.g.

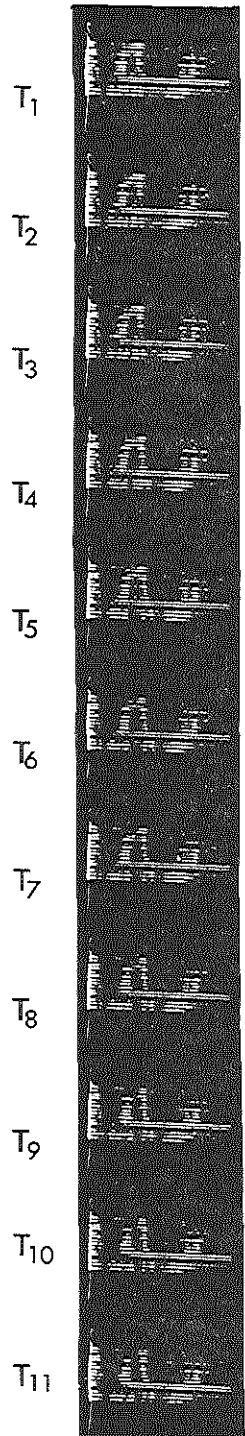


figure 4-9
Example of consecutive cardiac echograms at 40 milliseconds interval.

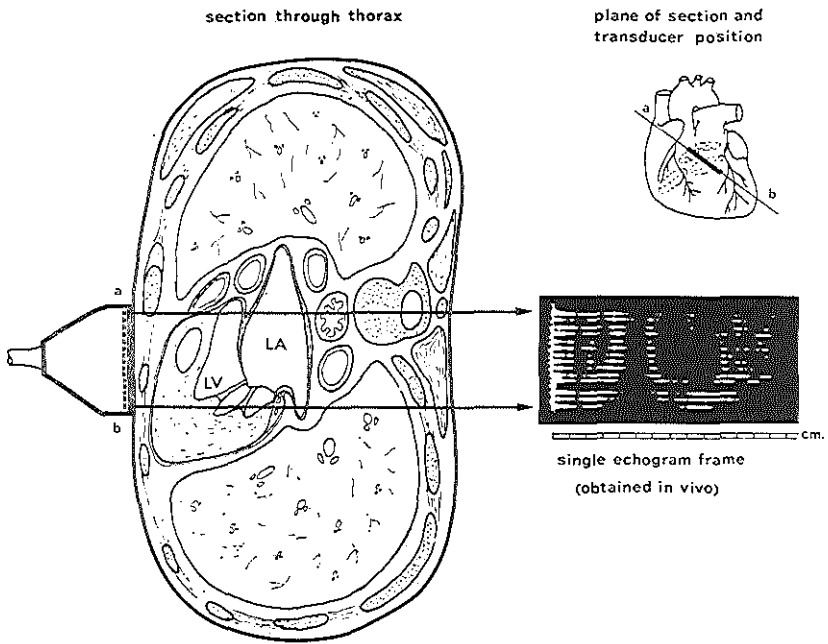


figure 4-10. Relation between transducer position, thorax and heart geometry and a resulting single frame echogram in a cross-section a-b.

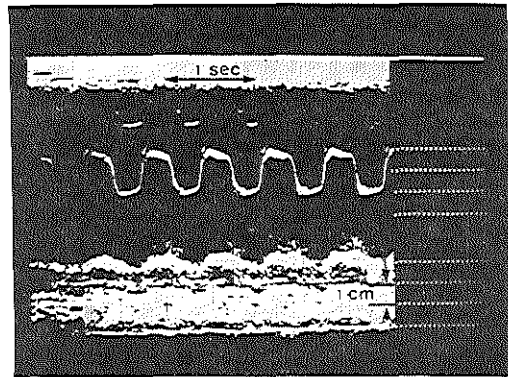


figure 4-11
Mitral valve u.c.g. obtained from the above discussed patient with severe mitral stenosis and mitral insufficiency. Distance between dotted lines is 1 cm.

From the same patient a recording was obtained with the transducer positioned as shown in figure 4-10. A single frame echogram obtained in section a-b and the reconstructed thoracic section show again the large left atrium and the left ventricular outflow tract with mitral leaflet. For comparison the conventional mitral u.c.g.-recording from the same patient is shown in figure 4-11. As a conclusion it may be stated that there is much to be learned in the interpretation of the above described data. It seems clear, however, that in near future a powerful diagnostic tool may become available to be added to the cardiological armamentarium.

CHAPTER V A CATHETER TIP INTRACARDIAC SCANNER

Summary:

In the previous chapter a new non-invasive echocardiographic method was discussed. It is the purpose of this chapter to introduce a 32-element catheter tip system (outer diameter 3 mm) specially developed for instantaneous study of moving cardiac structures during cardiac catheterization. The method is based on a phase-corrected circular array technique. A brief discussion on the preliminary results is given.

1. Introduction

As mentioned in the previous chapter non-invasive echocardiographic methods are subject to limitations caused by tissue and bone structures. These limitations include a restriction of transducer positions on the chest, a relatively long sound path and thus rather severe attenuation, and possibly incomplete acoustic coupling between transducer and chest. A catheter tip echo method carries the transducer into the heart itself. This would be advantageous in many respects. Virtually all cardiac structures come within close range of the tip, while no shielding by sternum, ribs, or lung tissue can occur. Good acoustic coupling between elements and blood is another positive aspect.

Catheter applications in cardiology continue to gain importance in clinical diagnosis (i.e. pressure transducers, fiber optics for oximetry and dye dilution and thermal dilution techniques). A recent innovation is the Swan-Ganz balloon catheter,²⁹ which "floats" into the pulmonary artery. With exception of fiber optics, none of these techniques can be used to visualize moving cardiac structures. Yet in the analysis of the function of the heart, continuous visualization of such moving structures would be of great importance.

A presently generally accepted method is the indirect visualization of the heart by fluoroscopy after injection of a contrast fluid in its cavities. Such "shadowgrams" will give the left ventricular outline while cine-angiocardigraphic recordings of these images permit the analysis of the contraction sequence of up to three cardiac cycles at a time. While better than "still" photographs, the need for repetitive injection of contrast medium and the toxic effects of prolonged radiation constitute

a severe limitation. It is envisaged that with the intracardiac scanner continuous information about the inside of the moving heart may be obtained, without any of these disadvantages.

Thus far several attempts have been made to obtain additional information about cardiac movements with various ultrasound catheter tip systems. Omoto⁷¹ describes a system whereby scanning of the inside of the heart was attained by mechanical rotation of a catheter with a single directional ultrasound element. Carleton et al⁷² used a non-directional cylindrical catheter tip element. The approximate cardiac diameter was derived from the echo travel time. Eggleton et al⁷³ used a 4-crystal catheter. This system depends on a stable state of the heart so that each beat is characteristic. By rotating the catheter and accumulating the data over many beats, a cross-sectional view in a selected "steady state" could be reconstructed. No system exists which provides a direct and continuous view of a complete moving cross-section. The need for such information stimulated the development of the method reported in this chapter.

2. The principle

It is known that phase compensated multi-element circular acoustic arrays are particularly well suited for fast rotation of the acoustic beam. Such a fast rotating beam could provide the instantaneous display of the desired cross-section without mechanical rotation of the catheter itself. Such devices have been described by James,⁷⁴ McCartney,⁷⁵ Fenby,⁷⁶ and others for sonar and radar applications. At the usually low maritime sonar frequencies these arrays are quite substantial (diameter in the order of a few meters).

The above-mentioned techniques could be made applicable to miniature high frequency arrays such as a multi-element catheter tip in the megahertz frequency range, if it were possible to build a corresponding miniature sonar array without loss of required acoustic properties.

In ultrasound techniques only the structures reflecting in the sound beam are displayed. For useful information, a "narrow" beam would therefore be advantageous. Since the directivity of the sound beam depends mainly on the geometry of the element and wavelength, these elements must have a prescribed size. Consequently, only a limited number of elements can be fitted to the catheter tip. With a small number of elements the data available to monitor all moving structures in an entire cross-section instantaneously will remain limited. However, by combining

many small elements in the circular multi-element array technique it proved possible to obtain a directional beam, such as would result from one element which is relatively large compared to wavelength. At the same time multi-directionality becomes possible. The necessary phase combination can be obtained by means of appropriate time delays.

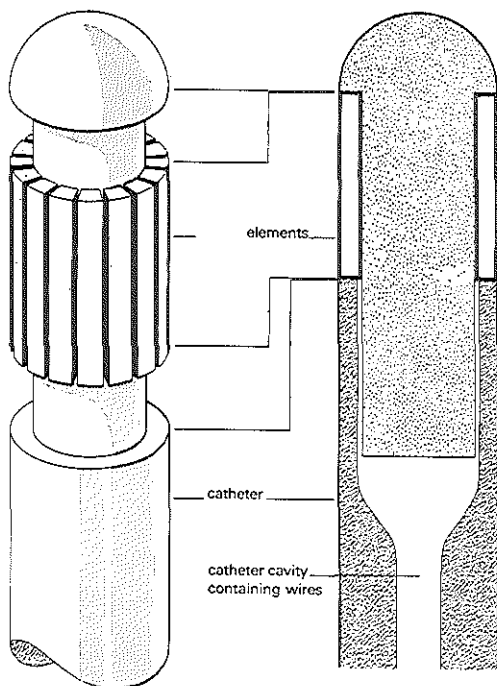
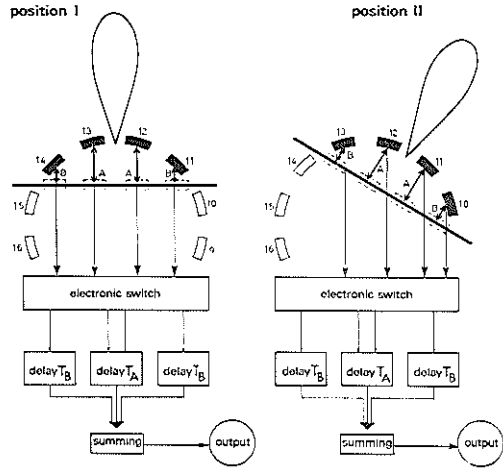


figure 5-1
Schematic drawing of 16-
element intracardiac catheter tip.

In figure 5-1 a schematic drawing of a multi-element catheter tip is shown. In figure 5-2 a simplified block-diagram is given together with a cross-section through the tip, in a plane perpendicular to the catheter length axis, where groups of small elements were activated successively. Since each element is small compared to the wave length no acoustic directionality can result if only a single element is used for transmission and reception of the acoustic pulse. If the incoming echoes of four elements were delayed as shown in figure 5-2, position I, the combined effects should result in an increased directionality. The same principle holds in transmission. The electronically inserted delays compensate for the acoustic travel time over distances A and B. The same situation applies to the adjacent overlapping subgroup of four elements due to rotational symmetry (figure 5-2, position II). The total number of beams from which directional information is obtained remains equal to the

figure 5-2
 Two consecutive scanning positions of 16-element catheter. The directivity pattern is formed using a 4-element combination (situation in receptive mode).



number of elements on the catheter tip. Thus information from many directions may be obtained. Fast electronic scanning and corresponding display results in an immediate image of the echo structure in the plane perpendicular to the catheter tip. Echoes are displayed radially from the centre on an oscilloscope screen. At each instant the radial direction corresponds to the direction of the transmitted acoustic pulse. The general block diagram is shown in figure 5-3 (see also figure 4-3).

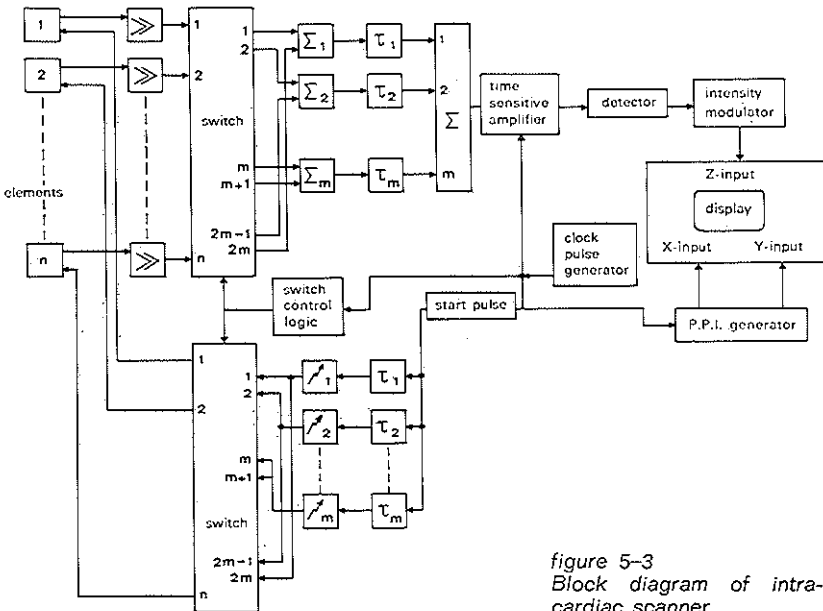


figure 5-3
 Block diagram of intra-cardiac scanner.

3. On the selection of parameters

In the initial evaluation of possible catheter applications and parameter selection, many unanswered questions, such as optimal frequency, dimensions, necessary minimum beam width, etc. were encountered. Development of the electronic system required knowledge about the combination of single elements and about the possible total number of elements on the catheter tip. As only limited knowledge was available, many parameters were selected on a rather intuitive basis with a strong emphasis on solutions given by practical considerations. They may be divided into three areas:

a. Limits due to medical considerations

In cardiac catheterization of patients, external maximum dimension of the catheter tip should not exceed a diameter of about 3 mm (French 9). This constitutes the major limit to the total number of elements on the tip.

b. Limits due to production problems

As may be seen in figure 5-1, the catheter is constructed first by bonding a cylindrical ceramic element onto a backing. In the next production phase single elements are cut from this cylinder. The remaining inter-element spacing is in the order of 0.13 mm. This puts constraints on the thickness of the cylindrical ceramic due to resulting single element thickness and remaining bonding area. For proper thickness vibration mode of the single elements a thickness/width ratio exceeding 2.5 has been chosen. It was found that, given an outer diameter of 3 mm, the production of 35 single elements on a catheter tip was possible if the frequencies were selected between 5 and 6 MHz. These above considerations led to the selection of barium titanate piezo-electric elements resonant at 5.6 MHz with a thickness of approximately 0.35 mm.

c. Acoustic and electronic limitations

At this point it became necessary to decide on the total number of elements in the array as well as on which cophasal combination from these elements should be selected as a practical optimum for directivity. The array diameter and the frequency range allowed, with the available delay lines, the combined use of cophasal elements on a limited arc of the circle only. The use of an element combination over a larger part of the circle would call for longer delays which in turn would result in a drop of the delay line cut off frequency. Even more important is that the acoustic screening from the backing material prevents the useful application of element combinations over the entire array. It was therefore decided to calculate the directivity pattern for various combinations of

phase corrected elements on arcs of approximately 90 degrees. Numerical calculations on parameter selection for optimal beam forming were carried out for catheter tip arrays containing a total of up to 64 single elements in the diametric plane only, and were limited to the far field zone. The details of these calculations are given in appendix F.

4. The directivity pattern

A directivity pattern represents the acoustic element sensitivity as a function of angle. Such a directivity function is only meaningful in the far field (see chapter II, section 2c). For the discussed catheter tip array in the plane of interest the gradual transition from near to far field occurs at about 2 mm distance. In practice directivity patterns have been measured at ranges from 2 to 6 cm. This distance corresponds in order of magnitude to inner ventricular size. Measurements were carried out with a small probe in a watertank as shown in figure 5-4. For the calculation of the array directivity pattern knowledge of single element radiation is important.

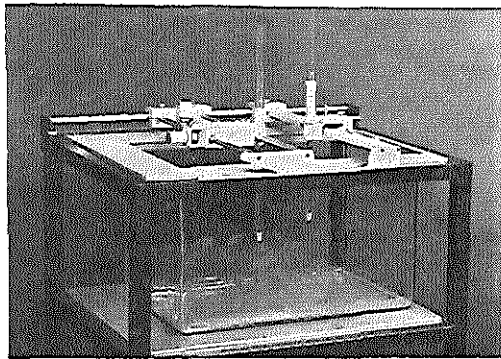


*figure 5-4
Model tank as used for in vitro measurements. The tank was constructed by the Central Research Workshop of the Medical Faculty Rotterdam.*

Since difficulties were envisaged in predicting the effect of bonding, sawing, soldering, etc. on mini-elements as well as the shielding effect caused by adjacent elements, only a crude approximation of single element radiation pattern was made. This radiation pattern has been approximated by the $\sin x/x$ function, where x depends on the wave number (see appendix F), the element width W and the directional angle. This function represents the directivity pattern of a continuous array of point sources with length W and thus neglects the curvature of the small elements. Furthermore, the screening effect of adjacent elements and backing material has been incorporated by the use of an angular attenuation factor. An impression of the variation in angular

sensitivity from element to element may be gained from figure 5-5, where the radiation pattern as measured from a multi-element catheter from a series of 11 adjacent elements has been shown. In figure 5-6 the average radiation pattern as derived from this series is compared to the single element approximation as used for array synthesis.

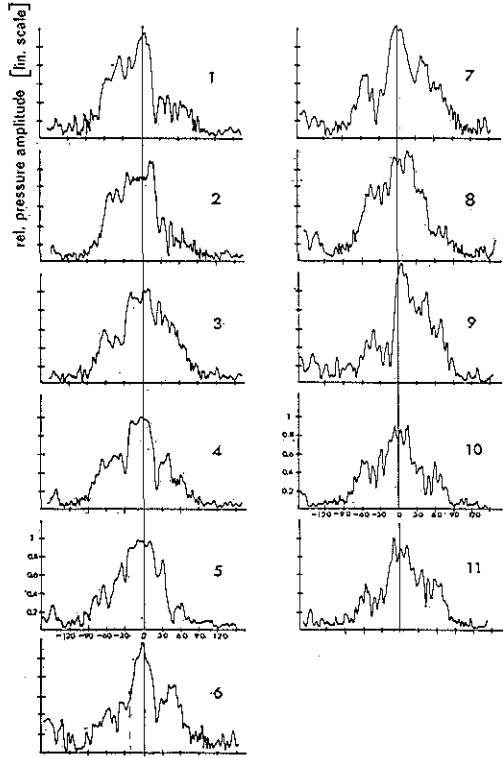


figure 5-5
Directivity patterns of a number of consecutive single elements from a 32-element catheter tip. Only amplitude information has been shown. No phase information is given.

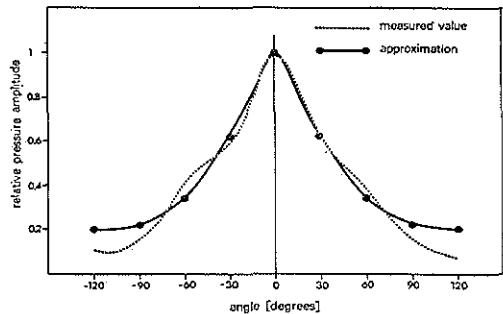


figure 5-6
Measured pressure amplitude averaged over eleven single elements, and calculated value as function of angle.

In a multi-element combination, phase information is very important (see appendix F). In practice the assumption that the single element phase was governed by the geometrical position of the element on the tip was found to be correct.

Some results of numerical calculations based on the described approximation are shown in figure 5-7. Major side lobes appeared particularly when the catheter tip arrays with low total element number were investigated.

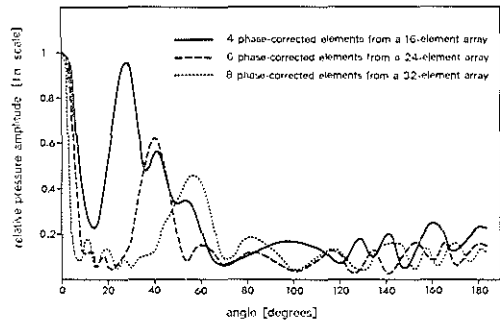


figure 5-7
Pressure amplitude as function of angle for 16-, 24-, and 32-element arrays. The directivity pattern of a cophasal element combination from elements on an arc of 90 degrees is given.

When the total number of elements increases, the angle between the main direction and the major side lobe increases and the side lobe becomes less pronounced.⁷⁴ As expected an array with a large number of elements should be aimed for. This has the additional advantage of an equally high number of “viewing directions”. These considerations led to the compromise of a 32-element catheter tip array with subgroups of 8 single elements for phase-corrected beam forming in 32 directions.

Four directions may be selected without any mutual overlap of element subgroups. It is to be expected that, if significant change in acoustic sensitivity were to occur, it will appear when the directivity of these 4 directions is compared. In figure 5-8 such a comparison has been shown. As may be seen the main lobe and side lobe characteristics do not change much (changes in the patterns for direction 32 have been caused by a short circuit between two elements).

As a further comparison the measured pattern of direction 8 and its calculated pattern have been shown in figure 5-9. Surprisingly enough the deviation is only small. Any catheters constructed thus far show the general directivity pattern behaviour as described. Apparently during production no essential change in the acoustic properties takes place. A further impression of the mechanisms of phase correction and directivity may be obtained from figure 5-10.

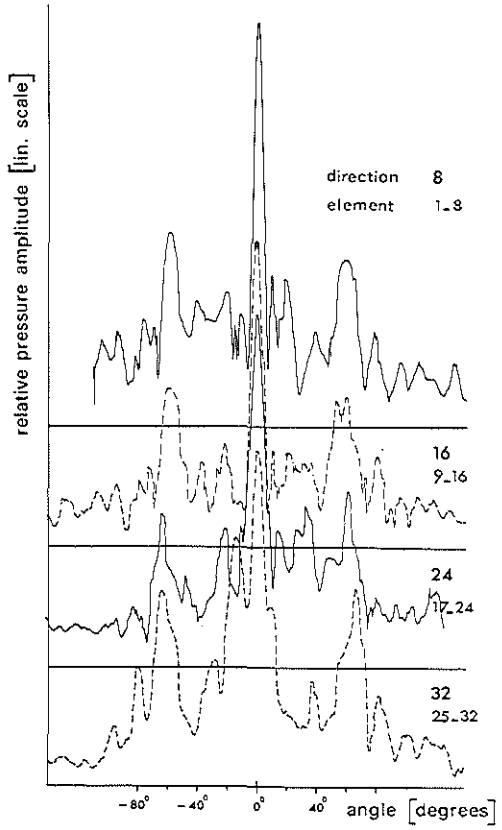


figure 5-8
Comparison of directivity
from different groups of 8
cophasal elements of a 32-
element catheter.

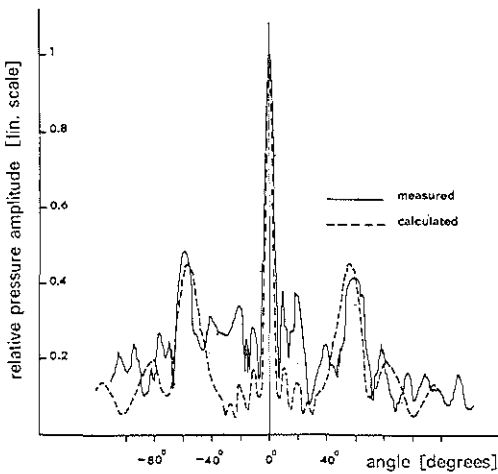


figure 5-9
Comparison of calculated
and measured directivity
patterns.

In figure 5-10 the result of an arbitrary subgroup of 8 adjacent phase-corrected elements as well as the summation of appropriately delayed pulses is shown. The summation has been shown for the main direction (position A) and for a direction where some individual elements do show the reception of an acoustic pulse, but the combined effect is almost zero (position B). Directionality is essentially identical in transmission and reception. If measured, due to measurement errors, small changes in directivity in transmission and reception will be present. In practice, the combined effect of directionality in reception and transmission will increase the directivity. Nevertheless, in the discussed situation, as a result of the two pronounced side lobes at about 58° the echogram may show two contaminating echo patterns.

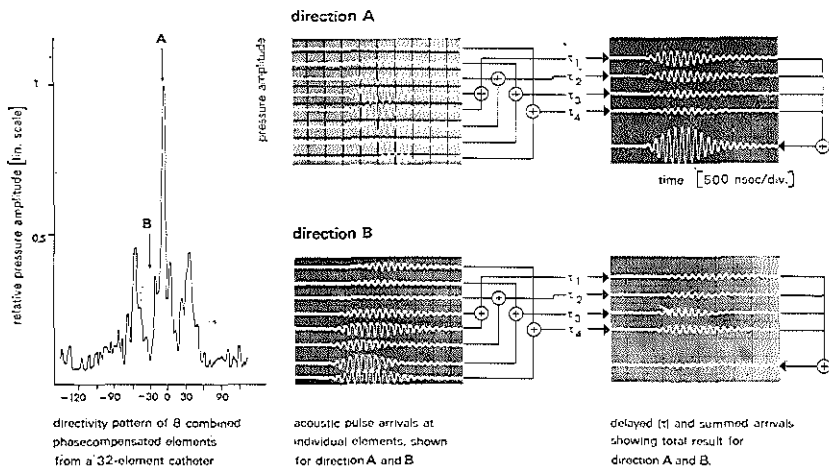


figure 5-10. Pulse arrival at 8 individual elements from two chosen directions in the combined directivity pattern.

5. Preliminary results

In figure 5-11 a photograph of a 32-element catheter tip over a millimeter grid is shown. The metal tip serves as common ground for the outer element electrodes. The ground wire as well as the individual element inner electrode wires are fed through the catheter cavity into the electronic apparatus.

If, for instance, the inner left ventricle is simulated by a cylindrical mesh reflector (see figure 6-6), figure 5-12 shows the echogram obtained. For this echogram the catheter and reflector were positioned in the water tank. Geometry of reflector and catheter tip has been shown in

the same illustration. From the echogram the asymmetrically positioned target is well recognizable. The small circle around the catheter tip position in the center of the echogram is caused by suppression of the transmission effect over the initial period.

Full depth scale has been set at 4 cm, but depth ranges of 2 and 8 cm may be selected as well. On the display the outer dots serve as a reference for this scale. One of the main features of this catheter system is the instantaneous display of reflector shapes. This is obtained with a full frame repetition frequency of 160 frames/sec. This repetition frequency is more than ample for human observation of moving structures. After a series of experiments future development will be aimed at suppression of side lobes.

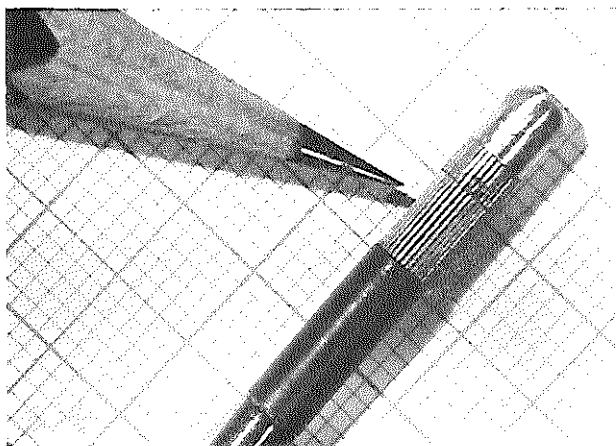
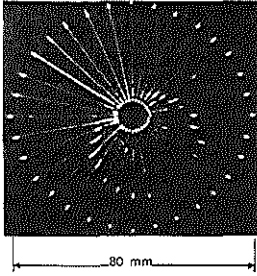


figure 5-11. Enlarged photograph of a 32-element catheter tip.

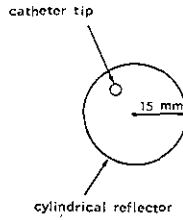
6. Concluding remarks

A first attempt has been described to apply phase compensated circular array techniques to a miniature multi-element catheter tip. It has been shown that a catheter with 32 elements and an outer diameter of 3 mm can be produced. This catheter has been designed as a diagnostic tool for immediate and continuous in vivo observation during cardiac catheterization.

This method should open a wide range of clinical applications. For instance, direct information on left ventricular size on a beat to beat basis becomes available. The same system may be utilized for continuous monitoring conditions as well. In addition several medical



ECHOGRAM



GEOMETRY

figure 5-12
Instantaneous echogram
obtained from a cylindrical
mesh target in a watertank.

applications outside the cardiovascular system as well as non medical uses can be envisaged.

A disturbance may be caused by the motion of the tip due to cardiac contraction. This will result in a shift of the echogram on the display. The influence and the severity of this effect will have to be evaluated in future experiments on animals. First experiences have been limited so far to the display of objects measured in the water tank.

CHAPTER VI ON THE LIMITATIONS OF ULTRASOUND

Summary:

After a discussion on specular reflection it is explained, by way of example, why in mitral leaflet motion recording the echo may vanish during part of the cardiac cycle. Next the influence of the chosen level of detection and amplification on range precision and axial resolution is explained. As a fourth topic, the reduction in lateral resolution due to substantial beam width and the effect of side lobes in the beam pattern on the echogram will be discussed. In both the non-invasive and the catheter tip diagnostic systems the zones from which erroneous echoes may arise have been calculated and measured for a circular reflector. The last part of this chapter is devoted to the Doppler effect.

1. Specular reflections

Angular dependence of reflection coefficients constitutes one of the limitations to proper understanding of diagnostic echograms. At a boundary, an ultrasound wave may be partially reflected. Just as in optical reflections, the angle of incidence and reflection are the same. Therefore, optimal echoes may be obtained only from structures approximately perpendicular to the sound beam. Since angles of incidence vary greatly in the heart, large variations in echo height exist. For instance, the echo of a small structure may appear large due to the fact that this structure happens to be perpendicular to the sound beam. Also, just as in optics, the nature of the reflecting surface is important. Reid⁶ measured the reflections from excised mitral valve leaflets as a function of angle of incidence. In healthy valve echograms a drop in echo amplitude by 50 % was noted, when the beam was rotated by as little as 5 degrees from normal incidence. Since the normal mitral leaflets may move through a considerable arc, the echo may sometimes vanish during part of the cardiac cycle. In a valve leaflet with a rough surface an appreciable echo was still obtained when the beam was rotated through an arc of 30 degrees. Apparently the recording of diseased leaflets was less difficult than the recording of normal leaflets. This agrees with clinical experience.

In order to overcome some of the deficiencies of specular reflection compound scanning may be employed (see chapter II). In this method the structure under observation is acoustically radiated from different directions. The echogram is made by integration in one display of the

information obtained from various directions. Proper synchrony between beam deflection and the aim of the transducer preserves correct geometrical information. Compound scanning is thus one of the tools by which the effect of unwanted specular reflections may be somewhat reduced.

2. Range precision and axial resolution

In most clinical investigations, the correct measurement of cardiac structure movement is looked for. This is possible by measurement of the change in the echo position. As echo position on the display may change slightly due to variation in the detector level setting, the echo distance need not correspond to true distance of the reflecting interface (see below). Since for the accurate understanding of movement actual distances are not relevant, relative position changes of one and the same echo are sufficient for high precision recording of cardiac movements.

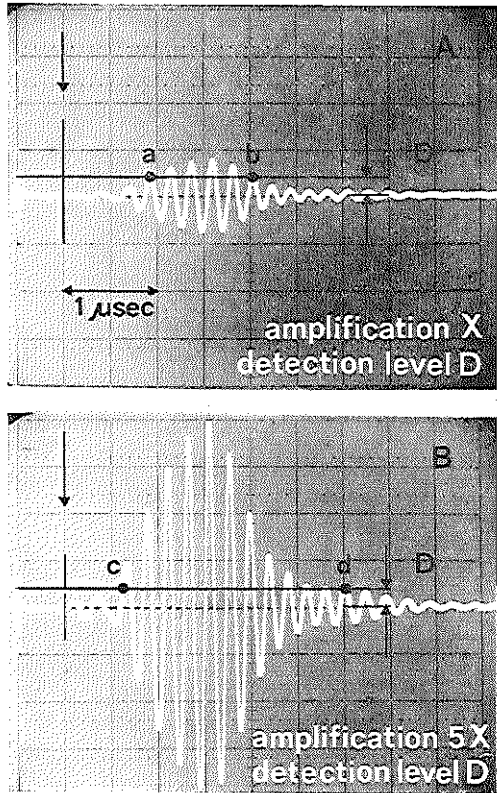
A different situation occurs when the purpose of the investigation is to reconstruct the two dimensional geometry or true distance between two structures. Here image distortion and incorrect distance measurement due to pulse length and dynamic range are some of the major difficulties.

a. Range precision

An echo is created at a boundary where two media with different acoustic properties join. Since this echo will have a certain length, the first recognizable part of the reflected sound wave is that part which exceeds the detection level selected for display. This part of the echo will be positioned at a point on the display which corresponds in depth to the structure just behind the echoing interface. Since there will always be some delay in time between the beginning of the actual echo from this boundary and the first point to appear on the display, certain restrictions on the accuracy of the depth measurement will have to be accepted. This above discussed deviation may be called the range precision.

In figure 6-1A, an echo has been shown measured from a thin reflector in the water tank. Figure 6-1B shows the same echo but with a 5 times greater amplification. The arrow marks the position of the thin reflector, and thus should indicate the beginning of the actual echo on the display. If the detection level is set at a value D and a low and high amplification respectively are chosen, the echoes in an intensity modulated A-scan show up as ab and cd . Obviously the range precision of a highly amplified pulse is better. This unavoidable deviation depends on the detection method, but is usually less than a few wave lengths (at 3 MHz wave length is 0.5 mm).

figure 6-1
Echo arrival from a thin
reflector shown for two
amplification settings.

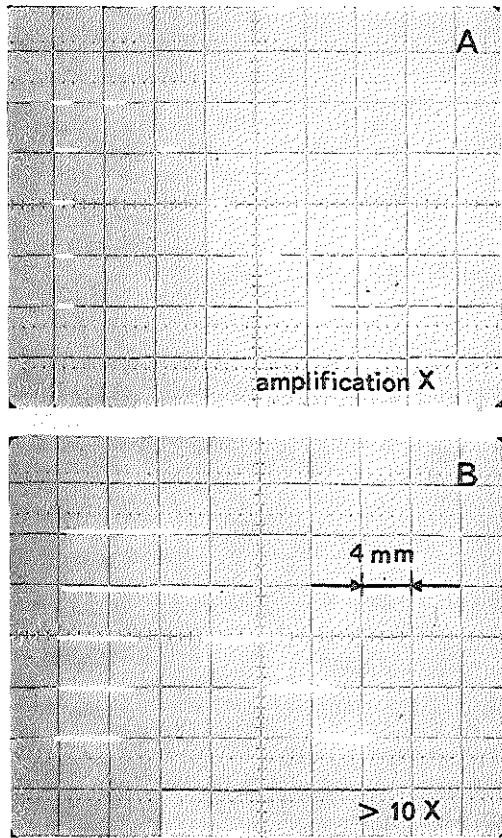


b. Axial resolution

Axial resolution may be defined as the minimum axial distance at which two reflecting structures may be recognized as separate entities. With low amplification (figure 6-1A) the detector setting would result in an echo width of ab . Without further processing any other echo arriving during period ab , cannot be distinguished. With high amplification this period is even longer. It is clear that an improvement in range precision is offset by an increase in echo length and therefore a decreased axial resolution. In figure 6-2 the intensity modulated echogram from two thin reflectors is shown with high and low amplification.

Each photograph shows repeated exposures of the two reflectors at 5 successively increased distances. As will be seen, the effect of high amplification on axial resolution is considerably greater than that on range resolution. As a further illustration the echogram of a circular object has been schematically drawn for short and long pulses.

figure 6-2
Echoes from two thin re-
flectors positioned at vari-
ous distances for two am-
plification settings.



This is shown in figure 6-3A and B respectively, for the non-invasive apparatus described in chapter IV. Long pulses tend to create a distortion of the ultrasound image. Optimal accuracy for distance measurement is obtained when only c is measured. This is exemplified by the echograms of aortic slices (see figure 4-7, where dotted area indicates distortion due to pulse length). The same situation would apply when intracardiac distances are measured from Time-Motion recordings.

Distance measurements between several structures and derived measurements such as those which are used in stroke volume calculations are subject to the above described errors. For example, a solid septal echo may be made up from two echoes merged due to long apparent echo lengths, whereas in fact two boundaries are crossed and two echoes should have been defined. Under these conditions precise estimation of internal left ventricular diameter may not be possible.

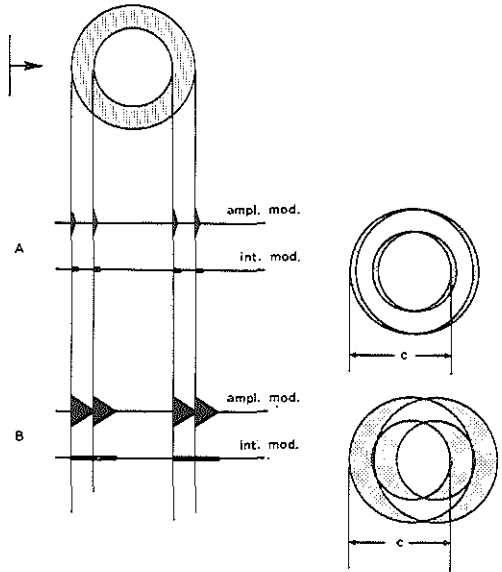


figure 6-3
Schematic construction of aortic echogram in the situation of short and long pulses.

3. Lateral resolution and effects caused by side lobes

a. Lateral resolution

Lateral resolution is defined as the minimum lateral distance between two reflectors which can be differentiated and visualized on the display. The shape of the acoustic beam is described by its directivity pattern. Since the directivity pattern and thus the width of the dominant beam is a function of frequency and element geometry, lateral resolution will depend on these parameters. Due to widening of the dominant sound beam with increase of depth lateral resolution will decrease with depth.

As a result distortion due to this effect is more apparent in areas far away from the transducer face. With 3 mm diameter, disk-shaped, piezoelectric elements, which resonated at a frequency of 3 MHz the beam width at 3 cm depth was measured to be 5.2 mm, whilst at 6 cm depth this width became 10 mm. In this case beam width was defined as the lateral distance between two points where the intensity was half the main axis intensity.

In conclusion it appears very important to understand the mechanisms to which two-dimensional echograms are subject and to realize that for optimal results all factors influencing pulse length require continuous attention.

b. Side lobe effect in the non-invasive system

A closely related limitation is the disturbance on the display caused by the effect of echoes from side lobe beams. Errors occur particularly when an echo is displayed as if resulting from the main beam direction, whereas it originated from a reflector in a side lobe direction.

In the non-invasive system (see chapter IV) various transducer frequencies are employed. The directivity pattern measured in the transducer plane of a single 4.5 MHz element is shown in figure 6-4.

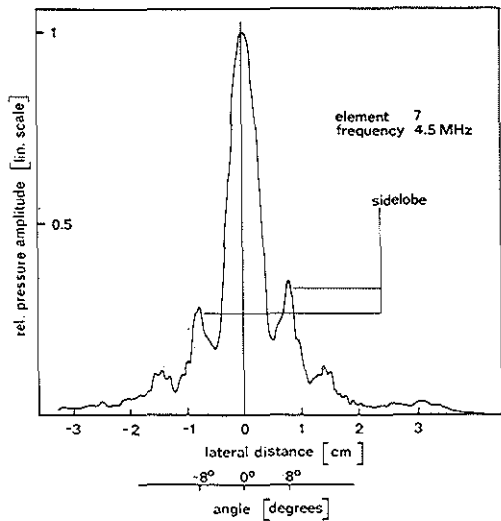


figure 6-4
Directivity pattern in transducer plane measured by lateral movement of a small probe at 6 cm distance.

In this transducer the first side lobes are positioned at 8 degrees. As shown in Appendix E, their effect was calculated and demonstrated for the case of a circular reflector. The misleading side lobe echoes produce an ellipsoid echogram on the display. For a circular reflector positioned at 10 cm depth with diameter of 3.3 cm and the 4.5 MHz multi-element line transducer the positions of the potentially misleading echoes have been computed and are shown in figure 6-5. Figure 6-6 shows a photograph of a circular mesh reflector as used in the water tank.

The corresponding actually measured echogram from such a reflector is shown in figure 6-7. As may be seen from that illustration, in this particular situation, the effect of the side lobe distortion is negligible. However, under different circumstances the overall effect of the discussed distortion on echograms is often unpredictable.

figure 6-5
 Construction of position (dotted ellipses)
 where erroneous echo display may occur
 with line transducer and circular reflector
 (see appendix E).

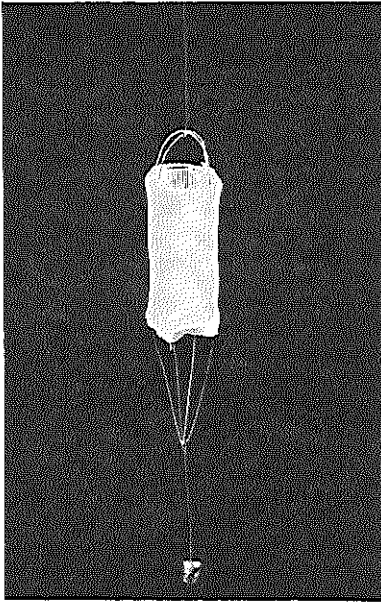
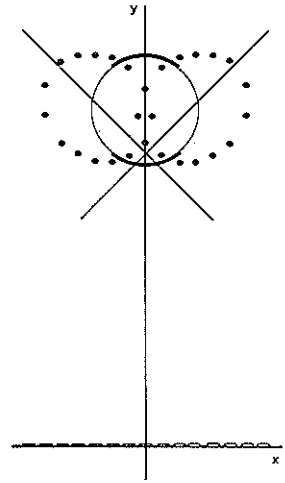
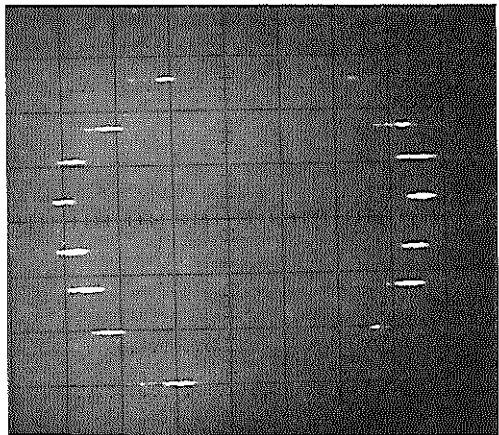


figure 6-6
 Circular mesh reflector as used for
 echogram studies.

figure 6-7
 Line array echogram from
 circular reflector with dia-
 meter of 3.3 cm (scale 0.5
 cm/div).



c. Side lobe effects in the intracardiac scanner system

In figure 6-8 the directivity pattern for an arbitrarily chosen group of 8 cophasal elements of a catheter tip (see chapter V) is shown. As may be seen the first important side lobes on either side of the main beam are larger than those shown for the line array side lobes in figure 6-4. This effect is added to the circular geometry of the catheter tip, which causes the superposition of three similar echograms, one obtained from the main beam, and two (mutually rotated) obtained from the side lobe directions. Therefore it can be anticipated that side lobe effects in this situation will be more pronounced.

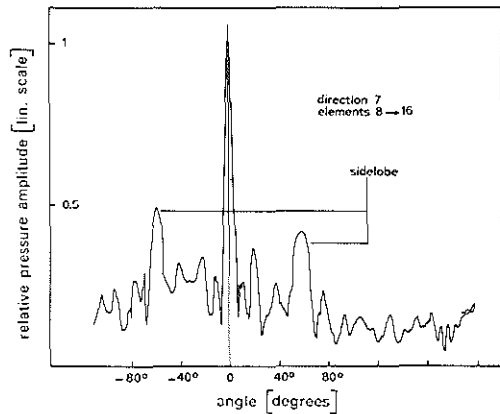


figure 6-8
Directivity pattern of 8 cophasal elements measured in a plane perpendicular to the catheter tip main axis.

With a catheter tip, positioned off center in a circular reflector, the zone where erroneous echoes may arise on the display has been constructed as shown in figure 6-9. For this, the correct echogram had to be rotated by approximately 58 degrees in either direction (side lobe directions; see figure 6-8).

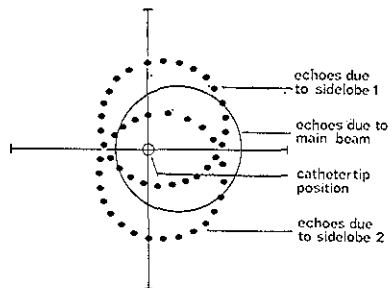


figure 6-9
Construction of position (dotted circles) where erroneous echo display may occur with catheter tip eccentrically positioned in a circular reflector.

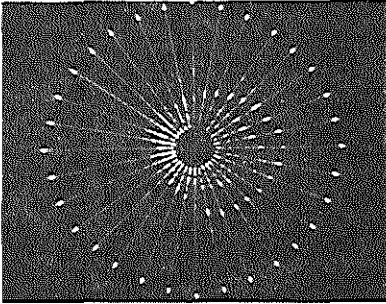


figure 6-10
Catheter tip echogram from an approximately circular reflector. The inner circle is caused by suppression of transmission transients.

In figure 6-10 the corresponding echogram has been shown with selected intensity setting resulting in slightly enhanced side lobe effect.

4. Limitations of continuous wave Doppler systems

With the aid of Doppler techniques exact velocities can be measured. They may for instance be used to measure the instantaneous maximum velocity in a blood vessel, and with a uniform velocity profile and a knowledge of vessel diameter, the volume flow may be obtained. Fahrbach⁷⁷ has discussed the necessary assumptions which would permit the measurement of volume flow (m^3/sec) under other conditions as well. The main points are:

– *Rotational symmetry of the velocity profile and laminar streaming.* Seed and Wood⁷⁸ measured the velocity profiles in the aorta in a study on animals. They found rather blunt profiles which showed skew during part of the cardiac cycle. Turbulent wave form was seen in only one case. In the aortic arch the entry conditions and curved geometry will almost certainly influence the velocity profile. Most Doppler measurements are, however, carried out transcutaneously at smaller, distal and "straight" arteries. Under these conditions the assumption of rotational symmetry and laminar streaming appears acceptable.

– *Homogeneity of scattering particles within the blood.* In his chapter "The radial displacement of blood particles in Poiseuille flow", Klip⁷⁹ describes the tendency of erythrocytes and other particles in an unaccelerated laminar flow to move away from the walls. It is not known to what extent this effect is present in the time varying flow in small vessels. If such an effect exists, it would influence the Doppler spectrum (see chapter II).

– *A frequency component from the Doppler spectrum should be proportional to the number of "scatterers" with corresponding velocity.* As described by Wells,¹⁰ when a separate transmitting and receiving element

is employed there is a region of maximum sensitivity on the central axis of the probe. This would tend to exaggerate the measured frequency shift caused by scattering particles from this region.

Provided the assumptions are correct, it has been shown (Oppenoorth⁸⁰) that for a parabolic velocity profile the frequency spectrum is flat. The highest frequency in the spectrum will be caused by the highest velocity. Rice⁸¹ derived a formula for the prediction of the average number of zero-crossings for a given spectrum. In the case of a flat spectrum, where the upper frequency limit is several times higher than the lower frequency limit, the average number of zero-crossings is directly related to the upper frequency limit. Furthermore, for a parabolic velocity profile, the average velocity over the cross-section is half the maximum velocity. Therefore, in this case, the measured value will be proportional to the average velocity over the cross-section. From this average velocity, volume flow may be calculated, if additional information about the inner vessel diameter is present. A further necessary parameter is the exact value of the angle of incidence between the sound beam and the vessel main axis.

Since in practice neither this diameter nor the velocity profile is known, a workable solution for clinical applications of apparatus based on the zero-crossing method would be to consider the time varying signal from the recorder to represent some average velocity over the lumen diameter. In this average the maximum velocity plays an important role. This measurement would be equivalent to the rather poorly defined "blood flow velocity" described in many papers on clinical Doppler applications. Clinical applications mentioned in chapter III must therefore be interpreted with caution, keeping in mind the restrictions identified above.

APPENDIX A THE MEASUREMENT OF ACOUSTIC RADIATION (The calibration of a sensor)

1. Introduction

Unfortunately detailed results concerning possible harmful effects of ultrasound on the heart are not frequent in the literature. However, Wells⁹² in his recent book "Physical Principles of Ultrasonic Diagnosis", which covers most of the ultrasound applications in medicine states: "Biological effects have been observed at intensities above 0.1 W/cm^2 , but not at intensities below 0.1 W/cm^2 ". This would indicate that, provided levels are below this maximum, applications of ultrasound may be without danger.

In order to obtain knowledge of the radiated intensities of the two devices discussed a calibration method had to be developed. Several methods for acoustic level measurement have been suggested in the literature and have been summarized by Carlin.⁸³ A comparison method with a calibrated sensor seemed the most practical solution for easy calibration.

This appendix describes the calibration of such a small sensor. The calibration was carried out at a frequency of 2.6 MHz on the basis of the effect of radiation pressure. A summary of the manifestations of radiation pressure under a variety of circumstances has been tabulated by Hueter and Bolt.⁵

2. Method of calibration

If radiated power is defined as the fraction of the acoustic energy per unit of time in the forward direction then this calibration procedure may be carried out as follows:

- a. Measurement of the acoustic output power P of a disk-shaped transmitter from its radiation pressure effect.
- b. Measurement of the relative intensity distribution in a plane S perpendicular to the main axis of the same transmitter at a given distance.
- c. Approximation of the lateral intensity distribution with an exponential formula and integration over S in order to calculate the output power P .
- d. Equation of the measured P value obtained in (a.) with a calculated value of P obtained in (c.) to yield Q (for Q see equation A-1). Knowing Q , the true intensity at a given point O of the acoustic field in front of the transmitter may be derived.
- e. Completion of the calibration procedure by placing the sensor in the above mentioned position O and obtaining the output voltage for the known local intensity.

3. The sensor

In order to avoid disturbance of the sound field the sensor should be small compared with wave length. The present calibration procedure has been applied to a commercially available Glennite probe, model UP-800 (see figure a-1). The dimensions of the sensitive element are given as 1.588 mm length x 1.47 mm diameter. The cylindrical shape of the sensitive element should provide non-directionality in the plane perpendicular to the cylinder main axis.

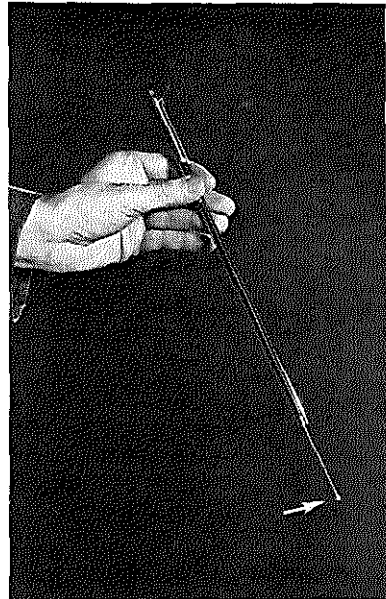


*figure a-1
Glennite Ultrasonic Probe UP-800.
The arrow indicates the sensitive
element.*

This would be advantageous since it obviates the necessity for careful aiming. However, since limitations in manufacturing determine the minimum dimensions of the sensor, the circumferential variations in the sensitivity do become apparent for high frequency ranges. It is therefore necessary to plot the directivity pattern of the sensor and to select one "calibration direction". In figure a-2 the directivity pattern at 2.6 MHz is shown.

4. Measurement of total output power

The effect of radiation pressure may be used to measure the radiated power of an ultrasound transducer. The design of presently available diagnostic echo sounders is based upon the transmission of short pulses and the reception of corresponding echoes. In such a system each short burst of high intensity ultrasound is followed by a relatively long dead zone. Due to the pulsed nature of the sound used, the average intensities

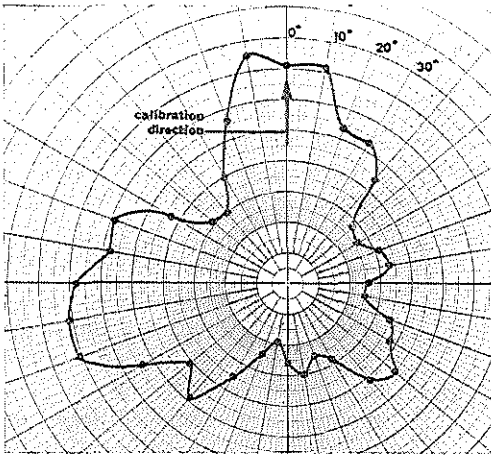


figure a-2
 Directivity pattern of the sensor showing pressure amplitude (lin. scale) as function of angle at 2.6 MHz.

will be very small. The integrated effect of radiation pressure on an absorber as measured with a micro-balance will therefore be very small. It is thus inconvenient to use a pulsed system for such a measurement and it becomes necessary to create a continuous ultrasound wave of relatively high power and use an absorber which should be large enough to intercept all radiated power. Rubberized hair was selected as the absorbing material. Measurements proved that the absorption was over 95 %. The radiated beam was directed into a water-filled absorber positioned on a micro-balance. The measuring accuracy of the micro-balance was 0.1 mg. The measurement set-up has been shown schematically in figure a-3. Switching the power on and off resulted in a change of apparent weight of the absorber. The difference as measured by a substitution method was used for further calculation.

5. Calculation of intensity in a single position

If the relative intensity distribution in a plane S perpendicular to the main axis of the transmitter at a distance D is known, then the integral of the relative intensity over the surface of the plane should be equal to the total radiated power. The equation gives the unknown scale factor for the calculation of true intensity. The geometry is shown in figure a-4. The transmitting crystal has a rotationally symmetric beam pattern so that it is sufficient to obtain the intensity distribution along a line.

The measured relative intensity distribution is shown in figure a-5. Kossoff⁶⁴ described the possibility of using a triangular approximation. Here a method with a distribution function according to Gauss was employed to approximate the shape.

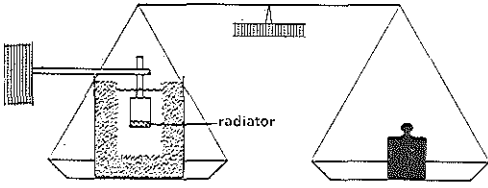


figure a-3
Schematic set-up of radiated power measurement.

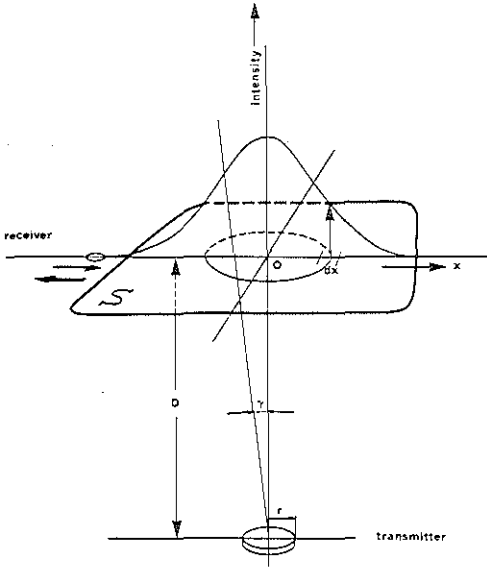


figure a-4
Geometry and symbols as used in the calibration procedure.

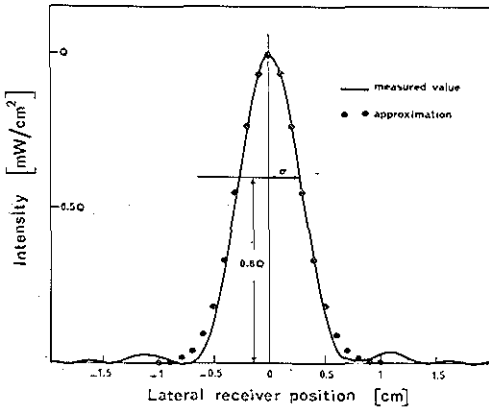


figure a-5
Lateral distribution of acoustic intensity at a distance $D = 10$ cm from the transmitter face. Frequency = 2.6 MHz. Transmitter radius $r = 5$ mm.

If lateral intensity distribution is given by $\exp(-x^2/2\sigma^2)$ then:

$$I_{true}(x) = Q \cdot e^{-x^2/2\sigma^2} = Q \cdot I_{rel}(x), \quad (A-1)$$

where Q is an intensity scale factor and σ is a scale factor in the x-direction. This approximation is shown as dots in figure a-5. As a next step we may establish the scale of the x-axis from the measured relative intensity curve by selecting the value of σ at the inflection points where $\exp(-x^2/2\sigma^2) = 0.6$.

In order to obtain the total radiated power P it is necessary to integrate over the surface S :

$$P = \int_S Q \cdot I_{rel}(S) \cdot dS, \quad (A-2)$$

due to rotational symmetry of I_{rel} this yields:

$$P = \int_0^{\infty} 2\pi x \cdot Q e^{-x^2/2\sigma^2} dx, \quad (A-3)$$

and reduces to:

$$P = 2\pi Q \sigma^2. \quad (A-4)$$

As P and σ are known, the factor Q can be calculated. If for calibration purposes the point of maximum intensity is calculated, the true intensity at this point is:

$$I_{max} = Q = \frac{P}{2\pi\sigma^2}. \quad (A-5)$$

The effect of radiation pressure as measured with a balance is due to the vertical force components only. If this effect is not taken into account, discrepancies may arise in the equation with the lateral intensity distribution. The introduction of the simple approximation of the intensity distribution gives rise to an additional error. In the calibration procedure described here the combined error due to above mentioned causes was found to be negligible (see appendix B).

6. Discussion of results

The sensor will give an output voltage proportional to the acoustic pressure. The relation between the pressure and corresponding acoustic intensity I , may be approximated by:

$$I = \frac{p^2}{\rho c}, \quad (\text{A-6})$$

p being the amplitude of the acoustic pressure (rms-value); ρ the density and c the sound velocity in the propagation medium. Assuming a linear relationship between the output voltage of the sensor and the measured pressure, a calibration graph showing output voltage against square root of intensity has been drawn through 4 calibration points in a commonly applied intensity range. For a number of frequencies these graphs are shown in figure a-6.

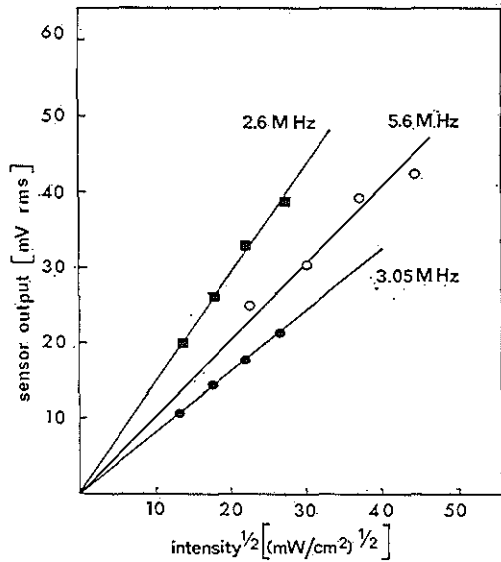


figure a-6
Calibration graphs of the sensor.

With these data it is possible to measure the intensity by placing the calibrated sensor tip in an unknown continuous acoustic field and converting the output of a rms-voltmeter using the graph in figure a-6. In an acoustic field of pulsed nature data such as peak intensity could be obtained by means of an oscilloscope. The acoustic radiation measurement of the 3 MHz transducer as discussed in chapter IV has been carried out using a calibration graph obtained with the method described above.

APPENDIX B THE MEASUREMENT OF ACOUSTIC RADIATION (The calculation of radiated power)

1. Introduction

In appendix A the calibration of a sensor was described. This calibration was based on the equation of measured radiated power and the calculated power derived from the integral over lateral intensity distribution.

Since the transmitting crystal radiated downward into a total absorber, the power is to be calculated by integrating the downward (axial) component of the intensity only. The intensity distribution was measured in a plane S perpendicular to the axis of the radiating crystal. Instead of the axial component, the measurement yielded the radial lateral intensity. Integration of the radial component over S would certainly not equal radiated power.

It was decided for practical purposes to calculate the radiated power from an approximation of the axial intensity. For this approximation of the axial lateral intensity by a normal function, the width of the measured radial intensity at 0.6 times maximum height was used. It is the purpose of this appendix to show that in doing so, the integral of the approximation over S is so close to the truly radiated power that the used calibration procedure may be assumed to be correct.

2. Calculation of radiated power

In practice no measurement of intensity distribution over a hemisphere was intended. As a theoretical example for further comparison, however, this situation will be discussed in this section.

As a start the theoretically correct value of the radiated power P is calculated. With a formula given by O'Neill⁸⁵ and with the assumption of rotational symmetry the radial intensity vector $I_{rad}(R, \gamma, \varphi)$ becomes:

$$I_{rad}(R, \gamma) = \frac{1}{2} \rho c \frac{u^2 K^2 s^2}{(2\pi R)^2} \cdot \left[2 \frac{J_1(a \sin \gamma)}{a \sin \gamma} \right]^2 \quad (B-1)$$

where $K = 2\pi/\lambda$ and $K \cdot r = a$

u = velocity amplitude at the crystal surface

r = radius of the transmitting crystal

λ = wavelength

s = transmitter surface

ρ = density

c = velocity of sound propagation

J_1 = Bessel function of order one

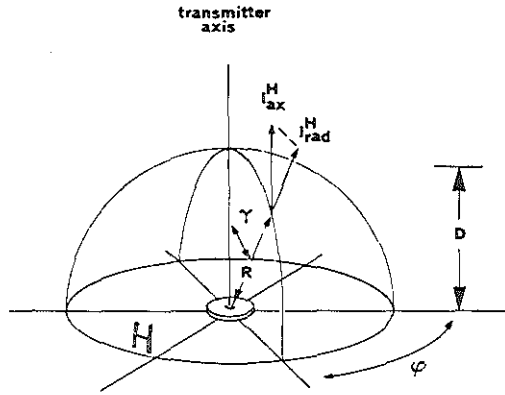


figure b-1
Schematic drawing of geometry.

The geometry is given in figure b-1, where H is the hemispherical surface with the transmitting element at its center. The power P radiating in the forward direction only, is given by:

$$P = \int I_{\text{rad}}(R, \gamma) \cos \gamma dH \quad (\text{B-2})$$

Integration over the hemispherical surface with radius $R = D$ and including $dH = D^2 \sin \gamma d\gamma d\phi$ we obtain:

$$P = \int_{\phi=0}^{2\pi} \int_{\gamma=0}^{\pi/2} I_{\text{rad}}(D, \gamma) D^2 \sin \gamma \cos \gamma d\gamma d\phi \quad (\text{B-3})$$

Substitution of equation (B-1) yields:

$$P = \int_{\gamma=0}^{\pi/2} \frac{\rho c u^2 K^2 s^2}{\pi} \cdot \frac{J_1^2(a \sin \gamma)}{a^2 \sin \gamma} \cos \gamma d\gamma \quad (\text{B-4})$$

Changing the variable of integration to $t = a \sin \gamma$ and using $a^2 = K^2 s / \pi$ gives:

$$P = \rho c u^2 s \int_0^a \frac{J_1^2(t)}{t} dt \quad (\text{B-5})$$

or:

$$P = \rho c u^2 s \left(\int_0^{\infty} \frac{J_1^2(t)}{t} dt - \int_a^{\infty} \frac{J_1^2(t)}{t} dt \right) \quad (\text{B-6})$$

the first integrale becomes:

$$\int_0^{\infty} \frac{J_1^2(t)}{t} dt = 1/2 \quad (\text{B-7})$$

introducing the constants C_1 and P_0 , such that:

$$\int_a^{\infty} \frac{J_1^2(t)}{t} dt = 1/2 C_1 \quad (\text{B-8})$$

and:

$$P_0 = 1/2 \rho c u^2 s \quad (\text{B-9})$$

the radiated power P yields:

$$P = 2P_0 \int_0^a \frac{J_1^2(t)}{t} dt \quad \text{or} \quad P = P_0(1-C_1) \quad (\text{B-10})$$

3. The approximation

For practical reasons it was decided to measure the intensity along a flat surface and from this derive the radiated power. The intensity was measured moving a small sensor along a straight line and squaring the measured acoustic pressure amplitude. Geometry has been shown in figure b-2.

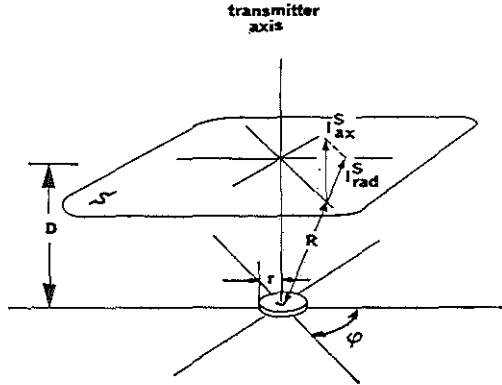


figure b-2
Schematic drawing of geometry.

Due to the predominant non directivity of the sensor the local measured intensity will be the radial intensity vector I_{rad} . If it is decided to measure the lateral intensity in a flat surface and the measuring technique records component I_{rad} instead of I_{ax} then the total radiated power P cannot be calculated from this recording by integration. It is therefore necessary to approximate the lateral intensity distribution with an adequately chosen function. Our purpose has been to find an approximating function $F(x)$ for the axial component with the following specifications:

1. Integrated over surface S it should yield the truly measured radiated power P . Thus:

$$\int_S F(x) dS = P \quad (B-11)$$

2. The parameters determining this function $F(x)$ should be easily obtainable from the recorded function $I_{S_{rad}}(x)$.

From a practical point of view the parameters should be limited to two, preferably a width parameter x_1 in the x-direction and a height indication y_1 as a parameter in the y-direction. In view of the shape of the

recorded curve a function corresponding with a normal distribution has been used as approximation. This yields:

$$F(x) = y_1 e^{-x^2/2x_1^2} \quad (\text{B-12})$$

It is now possible to calculate x_1 such that condition 1 holds. For the calibration procedure the width x_2 of the normal distribution has been obtained by measuring the recorded curve at 0.6 of maximum height (point of inflection). This value is introduced in equation (B-11) and (B-12) instead of x_1 . If this way of estimating x_1 is allowed, the ratio of x_1 and x_2 should be close to unity. By setting the height parameter y_1 equal to maximum height Q of the recorded curve, and $dS = x d\varphi dx$ the value of x_1 is defined by:

$$P = \int_S Q e^{-x^2/2x_1^2} dS \quad (\text{B-13})$$

This yields $2\pi Q x_1^2 = P$ or $x_1^2 = P/2\pi Q$.

If we recall that for $R = D$; $\gamma = 0$ and $\varphi = 0$ $I_{S_{\max}} = I_{H_{\max}} = Q$ we find:

$$I_{\max} = \frac{1}{2} \rho c \frac{u^2 K^2 s^2}{4\pi^2 D^2} \quad (\text{B-14})$$

and with use of equation (B-9):

$$Q = P_0 \cdot \frac{K^2 s}{4\pi^2 D^2} \quad (\text{B-15})$$

$$\text{or: } x_1^2 = \frac{P \cdot 4\pi^2 D^2}{2\pi P_0 K^2 s} = \frac{P_0(1-C_1) \cdot 4\pi^2 D^2}{2\pi P_0 K^2 s} \quad (\text{B-16})$$

with $K^2 s = \pi a^2$ we obtain:

$$x_1 = \frac{D}{a} \sqrt{2(1-C_1)} \quad (\text{B-17})$$

where C_1 is defined by equation (B-8). If we choose x_2 as the width of the recorded curve at 0.6 of maximum height, then x_2 is defined by:

$$\begin{aligned}
 & 4Q \cos^2 \gamma_2 \cdot \frac{J_1^2(a \sin \gamma_2)}{a^2 \sin^2 \gamma_2} = 0.6Q \\
 \text{and } & x_2 = D \tan \gamma_2
 \end{aligned}
 \quad \left. \vphantom{\begin{aligned} & 4Q \cos^2 \gamma_2 \cdot \frac{J_1^2(a \sin \gamma_2)}{a^2 \sin^2 \gamma_2} = 0.6Q \\ \text{and } & x_2 = D \tan \gamma_2 \end{aligned}} \right\} \quad (\text{B-18})$$

As a result we find:

$$\frac{x_2}{x_1} = \frac{a \tan \gamma_2}{\sqrt{2(1-C_1)}} \quad (\text{B-19})$$

As may be seen γ_2 and C_1 depend on the value of a . The ratio of x_2 and x_1 has been numerically calculated for the frequencies where calibration was carried out. The ratio was found to be close to one, therefore the described approximation method may be used.

APPENDIX C PERICARDIAL EFFUSION. CASE REPORT

(see figure 3-6 → 3-8)

The following is a case report of a patient in whom a pericardial effusion was diagnosed by means of ultrasound technique. The details of his course have been omitted but emphasis has been placed on left ventricular function studies to show the complimentary function of ultrasound studies in relation to techniques presently available during cardiac catheterization.

In June 1971 this 33 year old male patient was referred to the University Hospital in Rotterdam after his physician noted increase in cardiac size. A month earlier the patient noted tiredness and shortness of breath during exertion. In July he was admitted to the Department of Cardiology of the University Hospital Rotterdam because of increasing shortness of breath and a persistent cough for further diagnostic work up.

During examination a large heart was noted (see figure 3-6). There were increased venous pulsations in the neck indicating a disturbance in cardiac filling, and there was a pulsus paradoxus in the arterial pulse, i.e. an alternating volume of the pressure pulse related to the phase of respiration. This and the early diastolic heartsound, which was quite prominent, indicated impaired myocardial function. In addition there was a scratchy friction rub over the heart.

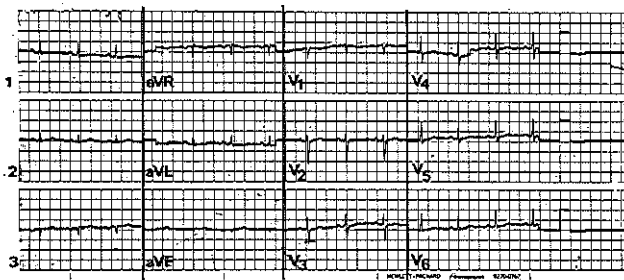


figure c-1. The 12-lead electrocardiogram as obtained from the patient with pericardial effusion.

The electrocardiogram (figure c-1) indicated decreased voltages of the QRS complex and also showed some minor changes in the S-T Segment of the electrocardiogram. Cardiac catheterization was carried out in September 1971. The results are summarized on page 81 in table I.

The most pertinent information was obtained from the angiocardigram which was obtained by filming with a 35 mm camera at 80 frames per second. The injection of contrast medium was given in the cavity of the



figure c-2. End-diastolic single frame angiogram obtained after injection of contrast medium in the left ventricle.



figure c-3. End-systolic single frame angiogram obtained after injection of contrast medium in the left ventricle.

left ventricle. In the two illustrations (see figure c-2 and c-3) an end-diastolic and an end-systolic frame are reproduced.

These two representative illustrations indicate not only a restriction in terms of absolute size, but also a marked degree of emptying indicative of an excellent capacity of the ventricle to empty itself in the face of a reduced capacity to fill. The respective values which were calculated for these volumes were an end-diastolic volume of 45 ml/m² (the normal is 70 ml/m² of body surface area) and an end-systolic volume of 9 ml/m² (versus a normal of 25 ml/m²). In other words the ventricle filled only up to 60 % of normal and emptied approximately three times as well as normal. The ejection fraction therefore was 80 % and resulted in a total stroke volume of 36 ml/m². The latter is a slightly depressed figure and corresponds with the reduced cardiac output usually found in patients with pericardial effusion under resting circumstances.

Further analysis of left ventricular muscle function demonstrated, both from the angiocardiographic data and from the data derived from the Telco micromanometer catheter inserted in the left ventricle, a high normal value for the index of contractility, V_{max} (see Hugenholtz et al,⁹⁹ Roelandt et al⁹⁸). This is an index reflecting the maximum contractile capacity of the unloaded cardiac muscle and is obtained by plotting the rate of change of wall stress or of pressure in the left ventricle against wall stress or pressure itself during isovolumic contraction. The data for V_{max} and also for the other indices of contractility such as peak dp/dt or peak V_{co} are all in the high normal range indicating an excellent muscle function.

The analysis of the cardiac catheterization data therefore shows:

1. A top normal or enhanced left ventricular muscle function.
2. A restriction to inflow of blood resulting in a decreased end-diastolic volume.

These data indicate that the healthy muscle was trying to compensate for the impaired filling caused by the constricting fluid in the pericardial sac by contracting more forcibly, and by emptying the ventricle to a greater extent in order to maintain cardiac output near normal.

The ultrasound cardiogram reflects these mechanisms quite clearly. The marked increase in excursion of the ventricular wall shown on figure 3-8 is indicative of an hyperactive contractile mechanism. In addition it shows the fluid between the ventricular wall and the anterior part of the pericardial sac. After the fluid was removed by pericardicentesis the cardiac shadow in the thorax is markedly diminished (see figure 3-7),

the hyperactive movements in the u.c.g. have disappeared, and cardiac function has been restored to normal (see figure 3-8). The patient is presently asymptomatic and has returned to work.

In this appendix the relationship between the conventional cardiac catheterization technique and the Ultrasound Cardiography Technique in both their applications is demonstrated. In this combined use of techniques the ultrasound A-scan permits a clear analysis of wall thickness and changes in wall contraction and a relatively easy detection of the presence of pericardial fluid.

General data:

age : 33 year	date : 1/9/71
length: 1.82 m	sex : male
weight: 78 kg	b. surface area: 2 m ²

Catheterization data:

	measured	normal	units
end diast. vol.	45	60-80	ml/m ²
end syst. vol.	9	15-35	ml/m ²
stroke volume	36	30-60	ml/m ²
ejection fraction	0.8	0.5-0.8	
cardiac output	5.8	> 4.5	l/min
cardiac index	2.9	> 2.5	l/min/m ²
heart rate	160	60-100	beats/min
dp/dt peak	2150	1500-2500	mmHg/sec
		(for k = 1)	cm ⁻¹
V _{max}	86	45-80	sec ⁻¹
V _{ce} peak	55	35-65	sec ⁻¹
L.V. diast. w. thickn.	0.8	0.8-1.3	cm
L.V. myocard. vol.	62	76-108	ml/m ²
L.V. weight	65	80-112	g/m ²

Table I: Data derived during cardiac catheterization for determination of left ventricular function.

APPENDIX D MITRAL STENOSIS. CASE REPORT

(see figure 4-8 → 4-11)

The following is the description of a patient with severe mitral stenosis in whom the disorder was detected by usual clinical methods and in whom it was also diagnosed with the conventional ultrasound A-scan. This was one of the first patients studied with the non-invasive cross-section viewer as described in chapter IV.

At a routine school examination, at age 14, this young female patient was found to have a cardiac murmur, and subsequently referred to the University Hospital Rotterdam. Because of increasing shortness of breath she was admitted, two years later, for a further diagnostic work-up to the Department of Cardiology.

On physical examination the pulse rate was 80 beats/min. and regular. The blood pressure was 110/85 mm/Hg. The heart was found to be enlarged to the anterior axillary line. A diastolic thrill was palpable at the apex. The thorax X-ray showed an enlarged heart with the left atrial shadow predominating. In figure d-1 the electrocardiogram is shown. This e.c.g. indicates a sinus rhythm with left atrial hypertrophy (V_1). The vectorcardiogram (Frank system) showed right and left ventricular hypertrophy.

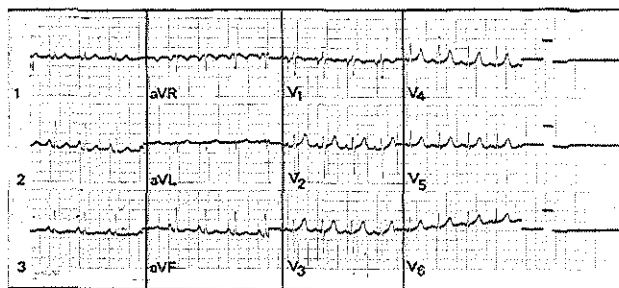


figure d-1. The 12-lead electrocardiogram as obtained from the patient with severe mitral stenosis and mitral insufficiency.

The phonocardiogram recorded at four different frequency responses with the e.c.g. and the apex cardiogram is shown in figure d-2. The findings confirm the auscultatory findings of a normal first heart sound, a gr. 2/6 holosystolic murmur and a gr. 4/6 diastolic crescendo murmur. These were all loudest at the apex. The second sound is soft, while an opening snap is present.



figure d-2. Phonocardiogram with ictus recording and e.c.g. from the patient with severe mitral stenosis and mitral insufficiency.

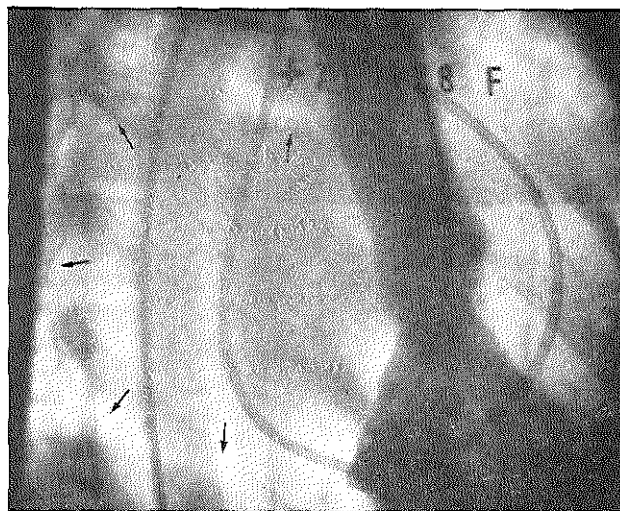


figure d-3. Single frame angiogram, in the right-anterior-oblique position, obtained after injection of contrast medium in the left ventricle (arrows indicate atrial outline).

Cardiac catheterization was carried out in december 1971. The relevant results are summarized in table II. The information obtained from the angiogram after injection of contrast medium in the left ventricle indicated gr. 3/4 mitral insufficiency manifested by rapid and complete filling of the left atrium by contrast medium coming from the left ventricle, a severely enlarged left atrium (see figure d-3) and a large but symmetrically contracting left ventricle.

The final diagnosis: severe mitral stenosis and mitral insufficiency. The patient is presently awaiting surgery.

General data:

age : 16 year	date : 8/12/71
length: 1.56 m	sex : female
weight: 47.4 kg	b. surface area: 1.3 m ²

Catheterization data:

	pressure in mm Hg				O ₂ sat. in %	
	phasic	normal	mean	normal	meas.	normal
right atrium	8/0	5/0	5	0-3	72	68-76
right ventricle	60/0/6	25/0/5			69	68-76
pulm. artery	60/30	25/10	50	12-18	70	68-76
pulm. art. wedge	30/20	10/0	25	3-6		96-100
left ventricle	110/0/5	100/0/5			96	96-100
aorta	110/80	100/60	100	70-90		96-100
mean d. valve grad.			22	0		

Heart rate: 110 beats/min.

Table II: Data obtained during left and right heart catheterization.

APPENDIX E SIDE LOBE EFFECTS OF A LINE TRANSDUCER ON A CIRCULAR REFLECTOR ECHOGRAM

As an example in this appendix the (first) side lobe effect for the multi-element line transducer discussed in chapter IV has been calculated. With a circular reflector the area of possible echoes due to this effect is shown to be positioned on two ellipses.

Let the x-axis coincide with the element row in the plane of the multi-element transducer as shown in figure e-1 for an arbitrary single element. With a circular reflector the echo from point $P'[x,y]$ will be erroneously displayed in $P[x_1,y_1]$. If $P'[x,y]$ represents an arbitrary point on the circular reflector which may be described by

$$x^2 + (y - y_0)^2 = r^2, \tag{E-1}$$

then $P[x_1,y_1]$ will be the displayed echo position whereby

$$\text{and } \left. \begin{array}{l} x_1 = x + y \tan \Theta \\ y_1 = y / \cos \Theta \end{array} \right\} \tag{E-2}$$

Reconstructing point P' from the $P[x_1,y_1]$ position calls for the expression of x and y in x_1 and y_1 . From equation (E-2) this results in

$$\text{and } \left. \begin{array}{l} y = y_1 \cos \Theta \\ x = x_1 - y_1 \sin \Theta \end{array} \right\} \tag{E-3}$$

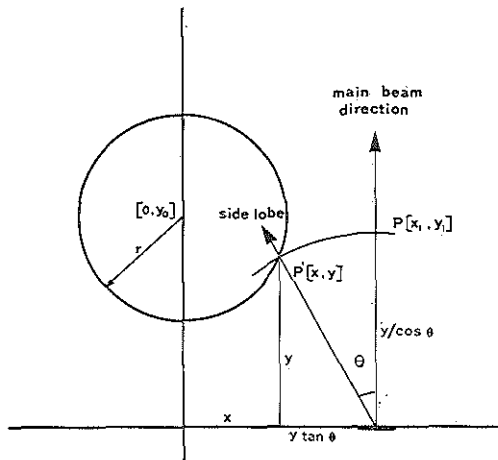


figure e-1
Geometry of erroneous echo display due to reflections from the direction of the side lobe.

Apparently $P[x_1 - y_1 \sin \Theta, y_1 \cos \Theta]$ is a point on the circle described by equation (E-1). We obtain therefore

$$(x_1 - y_1 \sin \Theta)^2 + (y_1 \cos \Theta - y_0)^2 = r^2 \quad (\text{E-4})$$

Equation (E-4) represents a quadratic function in the x-y plane. After some calculations equation (E-4) may be written as:

$$\frac{x^2}{r^2/(1 + \sin \Theta)} + \frac{y^2}{r^2/(1 - \sin \Theta)} = 1. \quad (\text{E-5})$$

Equation (E-5) represents an ellipse. In practice, if only the first side lobes are considered, the correct echogram of a circular object will thus be contaminated by an ellipsoidal echogram on either side.

APPENDIX F OPTIMUM BEAM FORMING FOR INTRACARDIAC SCANNER

As mentioned in chapter V, cylindrical arrays have the attractive feature that due to rotational symmetry any directivity pattern formed from such arrays may be rotated in the diametric array plane. Thus it is possible to rotate the beam rapidly without rotation of the array itself. In the case of the discussed catheter tip array, the length of the elements is 5 mm. It is felt that such elements will have sufficient directivity at right angles to the array plane to confine the sensitivity to near this plane. The following discussion is limited to directivity patterns in this plane only.

The major aim of pattern analyses is to limit the pulse transmission area as well as the acoustic sensitivity in reception to a well defined narrow region by careful selection of parameters. Without such an optimization ambiguity in the echo display will result (see chapter VI). Thus an optimal directivity pattern will show a narrow main beam as well as reduced side lobes. Since in reception and transmission beamforming is essentially the same we will limit the further discussion to reception only.

The synthesis of circular array patterns is a rather difficult subject. Some aspects have been described in literature.^{74,75,76,86,87} The following parameters will effect the directivity pattern:

1. diameter of the array in wave lengths
2. total number N of elements on the array
3. number of adjacent elements used for beam forming
4. single element directivity pattern
5. inserted phase compensation
6. amplitude variation around the array.

In order to facilitate parameter selection, a computer program has been developed (see flow chart at the end of this appendix). The program served to calculate numerically the influence on the directivity pattern of dimensions, number of elements, chosen frequency and amplitude weighting. Patterns are calculated by addition of signals from different elements with proper amplitude and phase. No correction for the pulsed nature of echo signals has been made, but since each pulse contains many periods, the transient effects will be small.

The single element directivity pattern was approximated by the well-known directivity function of a rectangular sensor with proper width. Thus the curvature has been neglected which seems reasonable for small elements. The selected width depends on production technique and for the examples in this appendix has been chosen 130 micron. In

an early stage it was possible to saw just one single element from a mounted ceramic cylinder on the catheter tip with loss of adjacent ones. Measurements on those single elements showed a decrease by a factor 0.2 in sensitivity for a change of 180° from the main beam direction. On a purely empirical basis such attenuation was incorporated by use of an exponential, angle dependent, factor in the single element directivity pattern.

For the fundamental case of phase corrected omnidirectional single elements, where the elements are uniformly driven, and spacing is relatively small, the resulting directivity pattern $v(\Theta)$ is given by:

$$v(\Theta) = J_0(a) \tag{F-1}$$

- where: Θ = deviation from the main beam direction
- J_0 = Bessel function
- $a = 2Kr \sin \Theta/2$
- $K = 2\pi/\lambda$
- r = radius of the array

figure f-1
Directivity pattern of uni-
formly driven phase-cor-
rected elements from circ-
ular array. Element spacing
is small.

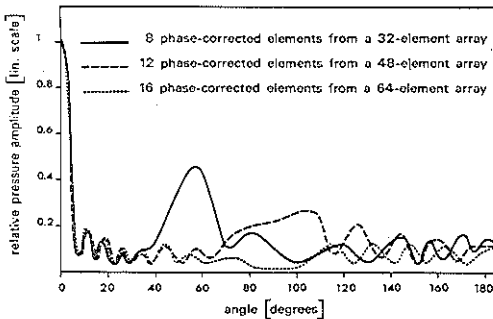
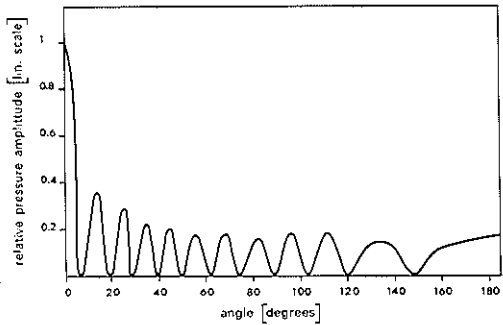


figure f-2
Side lobe behaviour for
various values of N. Where
N is the total number of
elements on the circular
array.

This radiation pattern has been shown in figure f-1 for a value of $Kr = 17.59$. In this figure the first side lobe appears at approximately 12 degrees with relative amplitude near 0.4.

Because of practical reasons we used only a limited number of single elements on an arc of the circular array. Since the elements have a finite spacing $> \lambda/2$, large side lobes appear (James⁷²). With the single element pattern approximation as discussed, the effect of parameter 2 and 3 upon the side lobe is shown in figure f-2.

Only elements on an arc of 90° were used for the pattern calculation. As already discussed in chapter V, the larger side lobe almost disappears for large N . Unfortunately an array with $N = 64$ could not be realised so far.

The effect on the side lobe of a modest increase of the number of single elements in a subgroup, is not necessarily favourable. It does, however, decrease the main beam width advantageously. This has been shown in figure f-3 for a value of $N = 32$.

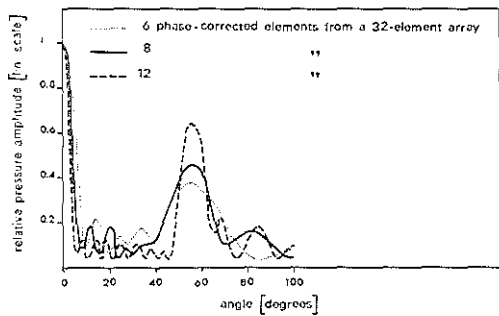


figure f-3
Influence on main beam width and side lobe behaviour with a variation of the arc length.

The effect of amplitude weighting in linear multi-element arrays is well understood.⁹⁸ Side lobe reduction is obtained at the expense of the narrowness of the main lobe. Amplitude weighting offers practical difficulties in circular array systems since for rotational use complex electronics would be required (in transmission). Despite the difficulties it seemed important to investigate whether amplitude weighting could possibly result in further reduction of side lobe effects.

The principle of pattern forming is based on the addition of acoustic waves from different elements with the proper amplitude and phase. In the cophasal situation in the main lobe direction the single elements have been phase corrected such that all contributions are equal in

phase. Obviously in the direction of a substantial side lobe, elements located in certain regions on the array contribute in phase. On other parts of the circle phase changes rapidly as a function of element position and no contribution is made. It is necessary to detect which element does contribute to a substantial side lobe. Reducing the weight of these elements might result in decrease of this side lobe at the

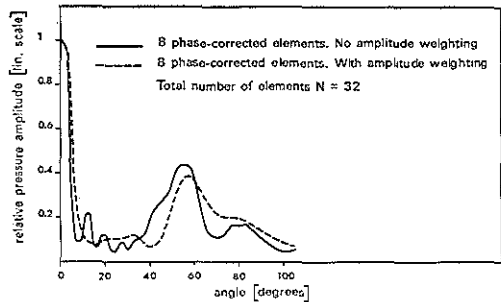
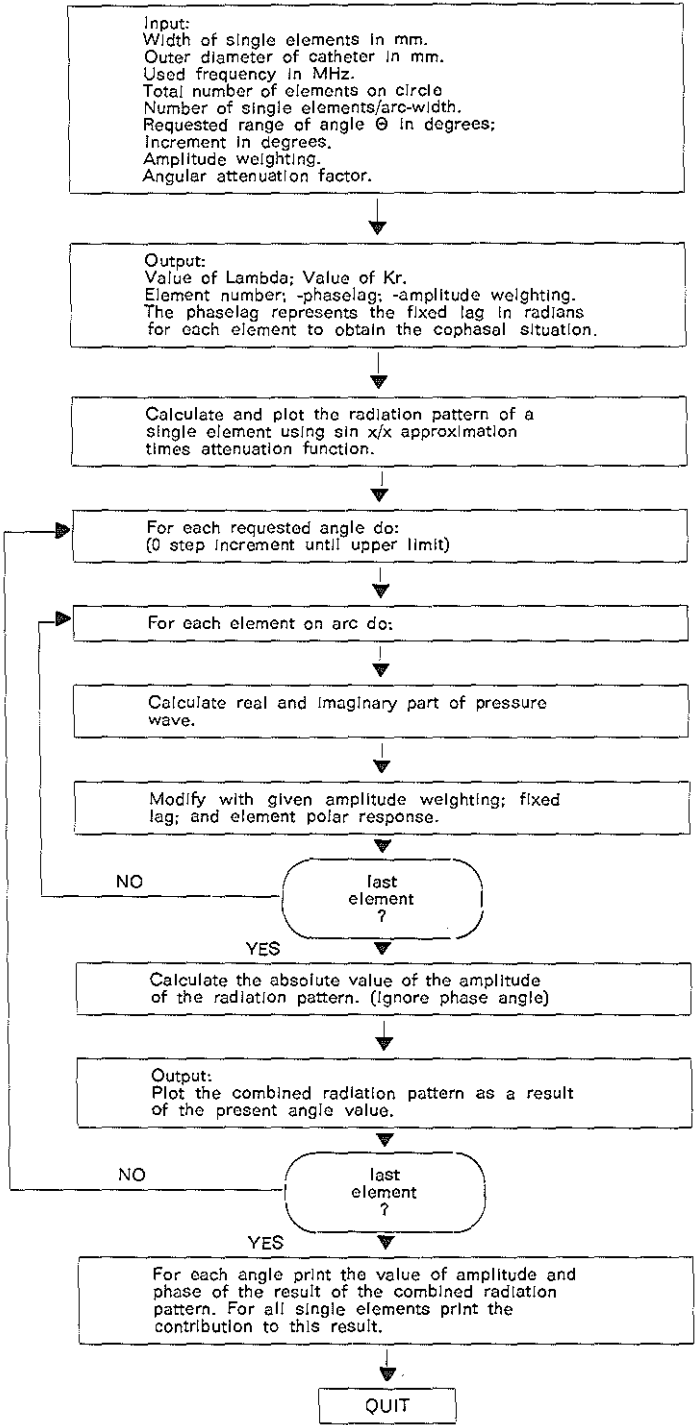


figure f-4
Influence of amplitude weighting on side lobe and beam width.

expense of main lobe narrowness. This principle is basically different from the normally used symmetrical taper in linear arrays.⁷⁴ In order to investigate such effects in circular arrays the program output contains the contribution of each single element to the total directivity pattern for each angle. Amplitude weighting has been applied for a variety of parameters. If weighting is used it should be applied to those elements which appeared to contribute most to that particular side lobe direction. If the directivity pattern was calculated using all single elements on the circle, an appreciable effect would result. If, however, only a smaller arc must be used no effective tapering can be carried out. This is shown in figure f-4.

For proper recognition of echo origin, understanding of beam forming is very important. As already mentioned in chapter V, the selection of parameters which influence the beam forming is in practice severely limited.

Yet, for further comprehension it seemed advisable to study different parameter combinations, and find out if a further improvement could be obtained. However, from these calculations it was decided to reject the amplitude weighting system. If, in future use, side lobes would turn out to have unacceptable consequences other signal processing techniques must be applied.



APPENDIX G POSSIBLE METHOD FOR DOPPLER MONITORING

Bendat⁹¹ and others have mentioned the detection possibilities of the zero-crossing rate and applications to communication theory and oceanography. Since the determination of the number of zero-crossings per unit time of a signal is inherently simple from the hardware point of view, it may be attractive to consider the passive detection of signals by this method.

As mentioned by Benchimol⁹⁶ it may be possible to use the vascular Doppler signal to monitor patients, for instance in a coronary care unit. It then becomes important to develop a simple processing technique that indicates a relative change in the spectrum.

A major contribution to the understanding of the zero-crossing theory was made by Rice⁹¹ who investigated the distribution of the zero-crossings (i.e. the crossings of the axis) of the stationary Gaussian noise function $y(t)$ and derived a formula for the population value, A , of the average number of zero-crossings per unit time:

$$A = 2 \left\{ \frac{\int_0^{\infty} f^2 W(f) df}{\int_0^{\infty} W(f) df} \right\}^{1,2} \quad (G-1)$$

where $W(f)$ is the spectral density function of $y(t)$. It is evident from equation (G-1) that a change in the shape of the spectral density function may lead to a change in the value of A . Thus in principle it would be possible in some cases to detect the change in spectral content by observing the zero-crossing rate.

Calculations show that, for instance, in the case of band-limited white Gaussian noise filtered in a 500–2500 Hz band and a sine wave frequency of 800 Hz a change in the counts/second from 3100 to 1600 occurs with a change in signal to noise ratio of 20 dB. Since the Doppler spectrum is usually down converted to the audio range it is suggested that these techniques may be useful in clinical patient monitoring. Initiation of such methods should be preceded by investigations into the possible biological effects of long term exposure of blood to continuous ultrasound waves.

REFERENCES

- ¹ Smyth, M. G.: *Animal Toxicity Studies with Ultrasound at Diagnostic Power Levels*, Diagnostic Ultrasound, Proceedings of the First International Conference, University of Pittsburgh, 1965, pp. 296-299.
- ² Kirsten, E. B., Zinsser, H. H., and Reid, J. M.: *Effect of 1 Mc Ultrasound on the Genetics of Mice*, IEEE Transactions on Ultrasonics Engineering, Vol. 3, December 1963, pp. 112-116.
- ³ Howkins, S. D., and Weinstock, A.: *The Effect of Focused Ultrasound on Human Blood*, Ultrasonics, July 1970, pp. 174-176.
- ⁴ Edler, I., and Hertz, C. H.: *The Use of Ultrasonic Reflectoscope for the Continuous Recording of the Movements of Heart Walls*, Kungl. Fysiografiska Sällskapets I Lund förhandlingar, Vol. 24, No. 5, 1954, pp. 40-58.
- ⁵ Hueter, T. F., and Bolt, R. H.: *Sonics*, John Wiley & Sons, Inc., 1966.
- ⁶ Reid, J. M.: *Ultrasonic Diagnostic Methods in Cardiology*. Thesis, University Microfilms, Inc., Ann Arbor, Michigan, 1965.
- ⁷ Franklin, D. L., Schlegel, W., and Rushmer, R. F.: *Blood Flow Measured by Doppler Frequency Shift of Back-Scattered Ultrasound*, Science, Vol. 134, August 1961, pp. 564-565.
- ⁸ Franklin, D. L.: *Techniques for Measurement of Blood Flow Through Intact Vessels*, Med. Electron. Biol. Engng, Vol. 3, 1965, pp. 27-37.
- ⁹ Satomura, S.: *Ultrasonic Doppler Method for the Inspection of Cardiac Functions*, J.A.S.A., Vol. 29, no. 11, November 1957, pp. 1181-1185.
- ¹⁰ Wells, P. N. T., *The Directivities of some Ultrasonic Doppler Probes*, Med. & Biol. Engng, Vol. 8, pp. 241-256.
- ¹¹ Goldberg, B. B.: *Suprasternal Ultrasonography*, JAMA, Vol. 215, No. 2, January 1971, pp. 245-250.
- ¹² Edler, I., Gustafson, A., Karlefors, T., and Christensson, B.: *Ultrasound cardiography, part II: Mitral and Aortic Valve Movements Recorded by an Ultra-Sonic Echo-Method. An Experimental Study*, The Department of Internal Medicine, University Hospital Lund, Sweden, pp. 68-82.
- ¹³ Effert, S., Bleifeld, W., Deupmann, F. J., and Karitsiotis, J.: *Diagnostic Value of Ultrasonic Cardiography*, British Journal of Radiology, Vol. 37, 1964, pp. 920-927.
- ¹⁴ Gramiak, R., Shah, P. M., and Kramer, D. H.: *Ultrasound Cardiography: Contrast Studies in Anatomy and Function*, Radiology, Vol. 92, No. 5, April 1969, pp. 939-948.
- ¹⁵ Gordon, D.: *The Use of Ultrasound in Diagnosis*, Ultrasonic Techniques in Biology and Medicine, Charles C. Thomas, Publisher, Springfield, Illinois, U.S.A., 1967, p. 139.
- ¹⁶ Kossoff, G., and Wilcken, D. E. L.: *The Cal Ultrasonic Cardioscope*, Med. & Biol. Engng, Vol. 5, 1967, pp. 25-32.
- ¹⁷ Schmitt, W., and Braun, H.: *Ultraschallkardiographie*, Georg Thieme Verlag, Stuttgart, 1970.
- ¹⁸ Edler, I.: *Ultrasound Cardiography*, Ultrasonics, April 1967, pp. 72-79.
- ¹⁹ Joyner, C. R.: *Experience with Ultrasound in the Study of Heart Disease and the Production of Intracardiac Sound*, Diagnostic Ultrasound, Proceedings of the First International Conference, University of Pittsburgh, 1965, pp. 237-248.

- ²⁰ Joyner, C. R., and Reid, J. M.: *Applications of Ultrasound in Cardiology and Cardiovascular Physiology*, Progress in Cardiovascular Diseases, Vol. 5, No. 5, March 1963, pp. 482-497.
- ²¹ Gustafson, A.: *Correlation between Ultrasoundcardiography, Hemodynamics and Surgical Findings in Mitral Stenosis*, American Journal of Cardiology, Vol. 19, January 1967, pp. 32-41.
- ²² Friedman, N. J.: *Echocardiographic Studies of Mitral Valve Motion. Genesis of the Opening Snap in Mitral Stenosis*, American Heart Journal, Vol. 80, No. 2, August 1970, pp. 117-187.
- ²³ Hertz, C. H., Edler, I.: *Die Registrierung von Herzwand Bewegungen mit Hilfe des Ultraschall-Impulsverfahrens* Acustica, Vol. 6, 1956, pp. 361-364.
- ²⁴ Feigenbaum, H., Zaky, A., and Grabhorn, L. L.: *Cardiac Motion in Patients with Pericardial Effusion*, Circulation, Vol. XXXIV, October 1966, pp. 611-619.
- ²⁵ Feigenbaum, H., Zaky, A., and Waldhausen, J. A.: *Use of Reflected Ultrasound in Detecting Pericardial Effusion*, American Journal of Cardiology, Vol. 19, January 1967, pp. 84-90.
- ²⁶ Joyner, C. R., Herman, R. J., and Reid, J. M.: *Reflected Ultrasound in the Detection and Localization of Pleural Effusion*, JAMA, Vol. 200, No. 5, May 1967, pp. 399-402.
- ²⁷ Werning, C. von: *Ultraschalldiagnostik in der Kardiologie* Archiv für Kreislaufforschung, Vol. 61, No. 2-4, 1970, pp. 139-159.
- ²⁸ Gibson, R., and Wood, P.: *The Diagnosis of Tricuspid Stenosis*, British Heart Journal, Vol. 17, 1955, pp. 552-562.
- ²⁹ Joyner, C. R., Hey, E. B., Johnson, J., and Reid, J. M.: *Reflected Ultrasound in the Diagnosis of Tricuspid Stenosis*, American Journal of Cardiology, Vol. 19, January 1967, pp. 66-73.
- ³⁰ Moreyra, E., Klein, J. J., Shimada, H., and Segal, B. L.: *Idiopathic Hypertrophic Subaortic Stenosis Diagnosed by Reflected Ultrasound*, American Journal of Cardiology, Vol. 23, January 1969, pp. 32-37.
- ³¹ Popp, R. L., and Harrison, D. C.: *Ultrasound in the Diagnosis and Evaluation of Therapy of Idiopathic Hypertrophic Subaortic Stenosis*, Circulation, Vol. XL, December 1969, pp. 905-914.
- ³² Pridie, R. B., and Oakley, C. M.: *Mechanism of Mitral Regurgitation in Hypertrophic Obstructive Cardiomyopathy*, British Heart Journal, Vol. 32, 1970, pp. 203-208.
- ³³ Shah, P. M., Gramiak, R., and Kramer, D. H.: *Ultrasound Localization of Left Ventricular Outflow Obstruction in Hypertrophic Obstructive Cardiomyopathy*, Circulation, Vol. XL, July 1969, pp. 3-11.
- ³⁴ Hernberg, J., Weiss, B., and Keegan, A.: *The Ultrasonic Recording of Aortic Valve Motion*, Radiology, Vol. 94, February 1970, pp. 361-368.
- ³⁵ Gramiak, R., and Shah, P. M.: *Echocardiography of the Normal and Diseased Aortic Valve*, Radiology, Vol. 96, July 1970, pp. 1-6.
- ³⁶ Pridie, R. B., Benham, R., and Oakley, C. M.: *Echocardiography of the Mitral Valve in Aortic Valve Disease*, British Heart Journal, Vol. 33, 1971, pp. 296-304.
- ³⁷ Winsberg, F., Gabor, G. E., Hernberg, J. G., and Weiss, B.: *Fluttering of the Mitral Valve in Aortic Insufficiency*, Circulation, Vol. XLI, February, 1970, pp. 225-229.

- ³⁸ Chapelle, M., and Mensch, B.: *Etude des Variations du Diamètre Ventriculaire Gauche chez l'Homme par Echocardiographie Transthoracique*, Arch. Mal. du Cœur, No. 11, 1962, pp. 1505-1517.
- ³⁹ Feigenbaum, H., Wolfe, S. B., Popp, R. L.: *Correlation of Ultrasound with Angiocardiology in Measuring Left Ventricular Diastolic Volume*, Amer. J. Cardiol., Vol. 23 : 111, 1969.
- ⁴⁰ Pombo, J. F., Troy, B. L., and Russell, R. O.: *Left Ventricular Volumes and Ejection Fraction by Echocardiography*, Circulation, Vol. XLIII, April 1971, pp. 480-490.
- ⁴¹ Pombo, J. F., Russell, R. O., Rackley, C. E., and Forster, G. L.: *Comparison of Stroke Volume and Cardiac Output Determination by Ultrasound and Dye Dilution in Acute Myocardial Infarction*, American Journal of Cardiology, Vol. 27, June 1971, pp. 630-635.
- ⁴² Popp, R. L., Wolfe, S. B., Hirata, T., and Feigenbaum, H.: *Estimation of Right and Left Ventricular Size by Ultrasound*, American Journal of Cardiology, Vol. 24, October 1969, pp. 523-530.
- ⁴³ Popp, R. L., and Harrison, D. C.: *Ultrasonic Cardiac Echography for Determining Stroke Volume and Valvular Regurgitation*, Circulation, Vol. XLI, March 1970, pp. 493-502.
- ⁴⁴ Feigenbaum, H., Popp, R. L., Chip, J. N., and Haine, C. L.: *Left Ventricular Wall Thickness Measured by Ultrasound*, Archives of Internal Medicine, Vol. 121, No. 5, May 1968, pp. 391-395.
- ⁴⁵ Heikillä, J. Tabakin, B. S., and Hugenholtz, P. G.: *Quantification of Function in Normal and Infarcted Regions of the Left Ventricle*, accepted for publication in cardiovascular research.
- ⁴⁶ Sjögren, A. L., Hytönen, I., and Frick, M. H.: *Ultrasonic Measurements of Left Ventricular Wall Thickness*, Chest, Vol. 57, No. 1, January, 1970, pp. 37-40.
- ⁴⁷ Inoue, K., Smulyan, H., Mookherjee, S., and Eich, R. H.: *Ultrasonic Measurement of Left Ventricular Wall Motion in Acute Myocardial Infarction*, Circulation, Vol. XLIII, June 1971, pp. 778-785.
- ⁴⁸ Kraunz, R. F., Kennedy, J. W.: *Ultrasonic Determination of Left Ventricular Wall Motion in Normal Man*, American Heart Journal, Vol. 79, No. 1, January 1970, pp. 36-43.
- ⁴⁹ Kalmanson, D., Veyrat, C., and Chice, P.: *Aspects Morphologiques de l'Onde de Flux Artériel Enregistrée par Voie Transcutanée chez le Sujet Normal*, Société Médicinale des Hôpitaux de Paris, Vol. 119, No. 9, 1968, pp. 743-752.
- ⁵⁰ Pourcelot, L.: *Application et Intérêt de l'Examen Ultrasonique par Effet-Doppler dans le Diagnostic Médical*, Université d'Orleans, Tours, Faculté de Médecine.
- ⁵¹ McDonald, D. A.: *The Relation of Pulsatile Pressure to Flow in Arteries*, J. Physiol, Vol. 127, 1955, pp. 533-552.
- ⁵² Strandness, D. E., and Sumner, D. S.: *Application of the Ultrasonic Flow Detector to the Study of arterial and Venous Disease*, 20th Annual Conference on Engineering in Medicine and Biology, November 1967, Mass., p. 27.5.
- ⁵³ Siegel, B., Popky, G. L., Mapp, E. M., Feigl, P., Felix, W. R., and Ipsen, J.: *Evaluation of Doppler Ultrasound Examination*, Archives of Surgery, Vol. 100, No. 5, May 1970, pp. 535-540.
- ⁵⁴ Allan, J. S., and Terry, H. J.: *The Evaluation of an Ultrasonic Flow Detector for the Assessment of Peripheral Vascular Disease*, Cardiovascular Research, Vol. 3, 1969, pp. 503-509.

- ⁵⁵ Woodcock, J. P., and Gosling, R. G.: *Transcutaneous Ultrasonics as an Alternative to Arteriography*, Proceedings of the British Institute of Radiology, Vol. 44, No. 523, July 1971, p. 562.
- ⁵⁶ Benchimol, A., Pedraza, A., Brener, L., Buxbaum, A., Goldstein, M. R., and Gartlan, J.: *Transcutaneous Measurement of Arterial Flow Velocity with a Doppler Flowmeter in Normal Subjects and in Patients with Cardiac Dysfunction*, Chest, Vol. 57, January 1970, pp. 69-78.
- ⁵⁷ Alexander, R. H., Nippa, J. H., and Folse, R.: *Directional Transcutaneous Assessment of Venous Inflow*, American Heart Journal, Vol. 82, No. 1, July 1971, pp. 86-92.
- ⁵⁸ Kalmanson, D., Veyrat, C., and Chiche, P.: *Atrial Versus Ventricular Contribution in Determining Systolic Venous Return*, Cardiovascular Research, Vol. 5, 1971, pp. 293-302.
- ⁵⁹ Rositano, S. A., and Sandler, H.: *Multichannel Doppler Blood Flow Measurement System*, 8th ICMBE, Palmer House, Chicago, Illinois, July 1969, Session 10-9.
- ⁶⁰ Baker, D. W., and Watkins, D. W.: *A Phase Coherent Pulse Doppler System for Cardiovascular Measurements*, 20th Annual Conference on Engineering in Medicine and Biology, November 1967, Boston, Mass., p. 27.2.
- ⁶¹ Flaherty, J. J., and Strauts, E. J.: *Ultrasonic Pulse Doppler Instrumentation*, 8th ICMBE, Palmer House, Chicago, Illinois, July 1969, Session 10-10.
- ⁶² Peronneau, P. A., and Leger, F.: *Doppler Ultrasonic Pulsed Blood Flowmeter*, 8th ICMBE, Palmer House, Chicago, Illinois, July 1969, Session 10-11.
- ⁶³ Åsberg, A.: *Ultrasonic Cinematography of the Living Heart*, Ultrasonics, april 1967, pp. 113-117.
- ⁶⁴ Pätzold, J., Krause, W., Kresse, H., and Soldner, R.: *Present State of an Ultrasonic Cross-Section Procedure with Rapid Image Rate*, IEEE Transactions on Bio-Medical Engineering, July 1970, pp. 263-265.
- ⁶⁵ Somer, J. C.: *Ultrasound Diagnosis, Progress Report*, Institute of Medical Physics TNO, August 1968, pp. 37-43.
- ⁶⁶ Ebina, T., Oka, S., Tanaka, M., Kosaka, S., Terasawa, Y., Unno, K., Kikuchi, Y., and Uchida, R.: *The Ultrasono-Tomography for the Heart and Great Vessels in Living Human Subjects by Means of the Ultrasonic Reflection Technique*, Jap. Heart Journal, July 1967, Vol. 8, No. 4, pp. 331-353.
- ⁶⁷ Tanaka, M., Neyazaki, T., Kosaka, S., Sugi, H., Oka, S., Ebina, T., Terasawa, Y., Unno, K., Nitta, K.: *Ultrasonic Evaluation of Anatomical Abnormalities of Heart in Congenital and Acquired Heart Diseases*, British Heart Journal, Vol. 33, 1971, pp. 686-698.
- ⁶⁸ Robertson, D. A. R., Hussey, M., and McDicken, W. N.: *Ultrasonic Time-Position and B-scanning of the Heart*, paper presented to the annual meeting of the British Medical Ultrasonics Group, Sonar in Medical Diagnosis, Glasgow, 1971, Abstract no. 5.
- ⁶⁹ Buschmann, W.: *New Equipment and Transducers for Ophthalmic Diagnosis*, Ultrasonics, January-March, 1965, pp. 18-21.
- ⁷⁰ Swan, H. J. C., Ganz, F. R. C. P., Forrester, J., Marcus, H., Diamond, G., Chonette, D.: *Catheterization of the Heart in Man with use of a Flow-Directed Balloon-Tipped Catheter*, New England Journal of Medicine, Vol. 283, No. 9, 1970, pp. 447-451.
- ⁷¹ Omoto, R.: *Ultrasonic Tomography of the Heart: An Intracardiac Scan Method*, Ultrasonics, April 1967, pp. 80-83.

- ⁷² Carleton, R. A., Sessions, R. W., and Graettinger, J. S.: *Diameter of Heart Measured by Intracavitary Ultrasound*, Medical Research Engineering, May-June 1969, pp. 28-32.
- ⁷³ Eggleton, R. C., Townsend, C., Kossoff, G., Herrick, J., Hunt, R., Templeton, G., and Mitchell, J. H.: *Computerised Ultrasonic Visualization of Dynamic Ventricular Configurations*, 8th ICMBE, Palmer House, Chicago, Illinois, July 1969, Session 10-3.
- ⁷⁴ James, P. W.: *Polar Patterns of Phase-Corrected Circular Arrays*, Proc. IEE, Vol. 112, No. 10, October 1965, pp. 1839-1848.
- ⁷⁵ McCartney, B. S.: *Proposals for an Electronically Scanned Circular Array*, Proc. IEE, Vol. 110, No. 7, July 1963, pp. 1220-1222.
- ⁷⁶ Fenby, R. G.: *Limitations on Directional Patterns of Phase-Compensated Circular Arrays*, The Radio and Electronic Engineer, October 1965, pp. 206-222.
- ⁷⁷ Fahrbach, K.: *Ein Beitrag zur Blutgeschwindigkeitsmessung unter Anwendung des Doppler Effektes*, Thesis, Fakultät für Elektrotechnik der Rheinisch-Westfälischen Technischen Hochschule Aachen, January 1969.
- ⁷⁸ Seed, W. A., and Wood, N. B.: *Velocity Patterns in the Aorta*, Cardiovascular Research, Vol. 5, 1971, pp. 319-330.
- ⁷⁹ Klip, W.: *Theoretical Foundations of Medical Physics, Volume II: An Introduction into Medical Physics*, University of Alabama Press, University Alabama U.S.A., 1969, p. 759.
- ⁸⁰ Opgenoorth, W. J.: *Dopplerflowmeting*, Report Technische Hogeschool Eindhoven, dept. of Electrotechnique, January 1970.
- ⁸¹ Rice, S. O.: *Mathematical Analysis of Random Noise*, Selected Papers on Noise and Stochastic Processes, Dover Publications, Inc. New York 1954, pp. 133-295.
- ⁸² Wells, P. N. T.: *Physical Principles of Ultrasonic Diagnosis*, Academic Press London-New York, 1969, p. 226.
- ⁸³ Carlin, B.: *Ultrasonics*, McGraw-Hill Book Company, New York, 1960, pp. 137-157.
- ⁸⁴ Kossoff, G.: *The Measurement of Peak Intensity Generated by Pulsed Ultrasonic Equipment*, Ultrasonics, Vol. 7, October 1969, pp. 249-251.
- ⁸⁵ O'Neill, H. T.: *Theory of Focusing Radiators*, J.A.S.A., Vol. 21, 1949, 516-526.
- ⁸⁶ Longstaff, I. D., Chow, P. E. K., Davies, D. E. N.: *Directional Properties of Circular Arrays*, Proc. IEE, Vol. 114, No. 6, June 1967, pp. 713-718.
- ⁸⁷ *Introduction to Sonar Technology*, Bureau of Ships-Navy Department-Washington, D.C., December 1965.
- ⁸⁸ Kraus, J. D.: *Antennas*, McGraw-Hill Book Company, Inc. Electrical and Electronic Engineering Series, 1950.
- ⁸⁹ Hugenholtz, P. G., Ellison, R. C., Urschell, C. W., Mirsky, C. W., and Sonnenblick, E. H.: *Myocardial Force-Velocity Relationships in Clinical Heart Disease*, Circulation, Vol. XLI, February 1970, pp. 191-202.
- ⁹⁰ Roelandt, J. R., Meester, G. T., and Hugenholtz, P. G.: V_{max} and $dP/dt/kP_{max}$ in Patients with Coronary Artery Disease (CAD) During Atrial Pacing (AP), Circulation, Supplement Number II, Vol. XLIV, No. 4, October 1971, p. 96.
- ⁹¹ Bendat, J. S.: *Principles and Applications of Random Noise Theory*, John Wiley & Sons, Inc., New York, 1958, p. 370.

SUMMARY

In the introduction, the purpose of this study as well as the principles of echocardiography (i.e. the use of ultrasound in cardiology in order to obtain data of diagnostic value) are briefly explained. Following this, in chapter II some physical properties of ultrasound and the clinically used recording techniques are discussed. These chapters serve to familiarize the reader with relevant aspects of ultrasound without providing details.

In chapter III an extensive review of the literature is given, and the important mitral valve motion technique and the ultrasound detection of pericardial effusion are discussed. Reference is made to clinical recordings obtained in patients.

Instantaneous two dimensional information of the moving heart may be obtained using multi-element concepts. A non-invasive, multi-elementary system is described in chapter IV. Results are shown obtained in vitro and in vivo. A catheter tip system is described in chapter V. Of this system in vitro results are given only.

The last chapter deals with limitations in ultrasound and particularly their effect on the above quoted systems. The literature seems to indicate that ultrasound – at diagnostic intensities – is harmless. In order to be able to compare radiated intensities from the present apparatus to quoted levels, a calibration method is described in appendix A and B.

Appendix C and D contain detailed case reports, while in E and F technical details on side lobe effects and beam formation are discussed. In appendix G a method for Doppler monitoring is suggested.

SAMENVATTING

In de inleiding wordt het principe van de echocardiografie (het gebruik van ultrageluid in de cardiologie voor het verkrijgen van diagnostische informatie) kort uitgelegd. Enige fysische eigenschappen van ultrageluid en de klinische registratiemethoden worden besproken in hoofdstuk II. Het doel van dit eerste gedeelte is om de lezer bekend te maken met enige aspecten van ultrageluid zonder hierbij op de details in te gaan.

Hoofdstuk III bevat een uitgebreid literatuuroverzicht. Tevens wordt verder ingegaan op de belangrijke mitraalklep-registratiemethode en de detectie van pericard effusie. Deze technieken worden besproken aan de hand van klinische registraties.

Door gebruik te maken van multi-element configuraties, is het mogelijk om direkt twee dimensionale informatie van het bewegende hart te verkrijgen. Een uitwendig multi-element systeem wordt besproken in hoofdstuk IV. Zowel in vitro als in vivo resultaten worden besproken. Hoofdstuk V bevat een beschrijving van een multi-element catheter tip systeem. Van dit systeem zijn de besproken resultaten beperkt tot in vitro metingen.

In het laatste hoofdstuk volgt een uitgebreide bespreking van de limitaties bij gebruik van ultrageluid, en in het bijzonder van deze effecten op de bovengenoemde systemen. Voorts wordt in appendix A en B een methode aangegeven om de uitgestraalde geluidsintensiteit te kunnen meten. In appendix C en D worden catheterisatiegegevens van twee patiënten met respectievelijk pericard effusie en mitraalstenose uitgebreid besproken. In appendix E en F worden details van het zijlob-effect en optimale richtingsgevoeligheid nader uiteen gezet. In de laatste appendix wordt een suggestie gedaan voor een mogelijke patiënt-bewakingsmethode gebaseerd op het Doppler-effect.

NASCHRIFT

Bij de totstandkoming van dit proefschrift heb ik veel medewerking ondervonden. Mijn dank hiervoor geldt in de eerste plaats Prof. Hugenholtz en Prof. Van den Brink voor hun voortdurende steun en belangstelling. Ook beide co-referenten, de heren ir. Van Wulfften Palthe en Dr. De Vlieger en voorts Dr. Laird, dank ik voor de door hen aan dit proefschrift geschonken aandacht.

Zonder de medewerking van alle leden van het Thorax Centrum en in het bijzonder van de heren ir. Lancée, Honkoop, Van Egmond en Van Zwieten bij het realiseren van de in dit proefschrift beschreven systemen zou dit werk onmogelijk zijn geweest. Bij de uitvoering hebben de Centrale Research Werkplaatsen onder leiding van ir. Bak aanzienlijke steun geleverd, o.a. op fijn-mechanisch en electronisch gebied.

Ten slotte zeg ik dank aan mevrouw Leusink en mevrouw Van der Jagt voor het teken- en typewerk.

CURRICULUM VITAE

Op aanbeveling van het college van dekanen volgt hier een korte levensbeschrijving van de auteur van dit proefschrift.

Hij werd geboren op 1 december 1937 te Velsen. Na de lagere school bezocht hij de toenmalige Hogere Burger School te Velsen waar het eindexamen werd afgelegd in 1955. Aansluitend werd het diploma van elektrotechnisch ingenieur behaald te Delft op 26 oktober 1961. De afstudeeropdracht (betreffende electro-magnetische golfpropagatie) werd uitgevoerd op de afdeling Theoretische Elektrotechniek onder leiding van Prof. Dr. ir. J. P. Schouten.

Als marine-officier werd de dienstplicht vervuld op het fysisch laboratorium van R.V.O.-T.N.O. te 's-Gravenhage. Daarna werkte hij gedurende ruim 5 jaar op het SACLANT research center in La Spezia, Italië. Op beide laboratoria lagen de werkzaamheden op het gebied van de onderwateracoustiek.

Sinds 1969 is hij onder leiding van Prof. P. G. Hugenholtz werkzaam op de afdeling Cardiologie van het Thoraxcentrum, Medische Faculteit Rotterdam. Als hoofd van de Echocardiografie-groep heeft hij sedert dien aan de in dit proefschrift vermelde systemen gewerkt.

This report is based in part on the following publications:

Bom, N., Lancée, C. T., and van Zwieten, G.: "*Calibration of an Ultrasound Sensor*", Ultrasonics 1971 Conference papers, pp. 73-75.

Bom, N., Lancée, C. T.: "*Algemene Inleiding tot de Echocardiografie*", the February 1972 issue of Het Ingenieursblad, Antwerpen.

Bom, N., Lancée, C. T., Honkoop, J., and Hugenholtz, P. G.: "*Ultrasonic Viewer for Cross-Sectional Analyses of Moving Cardiac Structures*", Bio-Medical Engineering, vol. 6, no. 11, november 1971, pp. 500-503, 508.

Bom, N., Lancée, C. T., and van Egmond, F.: "*Ultrasonic Intracardiac Scanner*", scheduled for publication in the March 1972 issue of Ultrasonics.

Bom, N., and Conolly, B. W.: "*Zero-Crossing Shift as a Detection Method*", Journal of the Acoustical Society of America, Vol. 47, No. 5, May 1970, pp. 1408-1411.

